Comparison of exact and numerical results in the XY model

D I P L O M A R B E I T

zur Erlangung des akademischen Grades
Diplom Physiker
(Dipl.-Phys.)

eingereicht an der
Mathematisch-Naturwissenschaftlichen Fakultät I
Humboldt-Universität zu Berlin

von
Tomasz Korzec
geboren am 28.11.1977 in Warschau

Präsident der Humboldt-Universität zu Berlin:
Prof. Dr. Jürgen Mlynek

Dekan der Mathematisch-Naturwissenschaftlichen Fakultät I:
Prof. Dr. Michael Linscheid

Gutachter:

1. Prof. Dr. Ulrich Wolff
2. Prof. Dr. Michael Müller-Preussker

eingereicht am:	31. Januar 2003
Tag der mündlichen Prüfung:	28. Februar 2003

Abstract

Exact predictions for the finite volume energy spectrum of the sine-Gordon model were presented recently. The derivation of these results invokes steps which are mathematically not entirely rigorous, so a confrontation with numerical results is desirable.

The two dimensional XY model is examined with Monte Carlo methods. It is believed to lie in the same universality class as the sine-Gordon model at a certain value of the sine-Gordon coupling. Several points of the step-scaling function are compared to each other. The predictions are valid for the continuum so an extrapolation from simulations at a finite lattice spacing a to $a = 0$ has to be performed. At the same time a prediction for the decay of lattice artifacts can be verified.

To extract the step-scaling function from the theoretical predictions it is necessary to solve nonlinear integral equations.

Efficient cluster algorithms and an improved estimator for the correlation function are applied in the simulations.

The thesis confirms the predicted form of the lattice artifacts as well as the continuum-predictions for the step-scaling function within statistical errors.

Keywords:
XY model, Monte Carlo, Destri-de Vega equation, lattice artifacts

Zusammenfassung

Es wurden neuerdings exakte Formeln für die Berechnung der Energieniveaus des sine-Gordon-Modells (im endlichen Volumen) vorgestellt. Die Herleitung der Resultate ist mathematisch nicht ganz rigoros, weshalb eine numerische Überprüfung wünschenswert ist.

Simuliert wird das XY-Modell in zwei Dimensionen. Man glaubt, daß es in der gleichen Universalitätsklasse liegt wie das sine-Gordon-Modell mit einem bestimmten Wert der sine-Gordon-Kopplung. Verglichen werden dann einige Punkte der step-scaling-Funktion. Die exakten Formeln gelten für das Kontinuum, deshalb muß erst aus den Simulationen bei endlichem Gitterabstand a auf $a = 0$ extrapoliert werden. Gleichzeitig kann überprüft werden, ob sich eine vorhergesagte Form der Gitterartefakte bestätigen läßt.

Um die step-scaling-Funktion aus den theoretischen Vorhersagen zu extrahieren ist es notwendig nichtlineare Integralgleichungen zu lösen.

Zur Simulation werden effiziente Cluster-Algorithmen sowie ein ,,improved estimator" für die Korrelationsfunktion verwendet.

Die Arbeit bestätigt sowohl die vorhergesagte Form der Gitterartefakte, als auch die Kontinuums-Vorhersagen im Rahmen der numerischen Genauigkeit.

Schlagwörter:
XY-Modell, Monte Carlo, Destri-de Vega Gleichung, Gitterartefakte

Contents

Chapter 1

Introduction

The XY model in two dimensions is a statistical system of classical spins located on the sites of a rectangular lattice. The spins are continous variables parametrized by an angle which gives their position on a unit circle. Originally this model was developed to describe the physics of ferromagnetic layers in a simple way. When in the late sixties the phenomenon of *universality* was explained in the framework of renormalisation group theory the XY model attained new attention.

At their critical points (e.g. the triple point of water) statistical systems exhibit a very special behavior. Certain physical quantities (e.g. the specific heat) loose their dependence on microscopic details like the special form of the interactions and depend only on properties like the dimensionality of space and the internal symmetries of the system. Many different systems show the same critical behavior. They are said to belong to the same *universality class*. This is why the study of critical points and phase transitions is so important.

The XY model exhibits a very specific phase transition which is of infinite order. Its nature was explained by Kosterlitz and Thouless [1]. Due to universality the XY model is suitable to explain the critical behaviors of many other systems. Amongst them are He^4 films where a transition to supra-fluidity occurs, surfaces of crystals in equilibrium with solutions (roughening transition), as well as the two dimensional Coulomb gas (transition from an insulator to plasma).

The second important application of the XY model is in the context of quantum field theories. Feynman's path integral formulation of quantum field theory made a connection between these theories formulated on an Euclidean space-time and statistical systems apparent. At the critical points of a statistical system where the correlation length becomes infinite, a field theory is recovered. In the case of the XY model it is the nonlinear $O(2)$ invariant $\sigma-$model. Thus studying the critical properties of the XY model teaches us a lot about the related quantum field theory.

Although the XY model and its phase transition have been known for at least thirty years some interesting new results related to the corresponding field theory were put forward recently. It was possible to give exact expressions for the energy levels of the $O(2)$ $\sigma-$model in the context of the *sine Gordon* model which for some particular choice of its parameters lies in the same universality class as the XY model. The derivation of these results includes some steps which are mathematically not entirely rigorous, therefore a numerical confirmation is desirable.

The main task of this thesis is to check numerically whether the predictions can be confirmed or not. A suitable quantity to investigate is the *LWW-coupling* [2] which is a measure of the finite volume massgap. The XY model is studied with Monte Carlo methods on the lattice. The LWW-coupling is extracted by measuring the correlation function of zero spatial momentum fields between different time slices. To obtain high precision results efficient cluster algorithms and an improved estimator for the correlation function are used.

In the extrapolation of the data to the continuum a new prediction for the decay of lattice artifacts is tested. The deviation of the coupling, measured on the lattice, from its continuum value is well described by an expansion in the inverse logarithm of the correlation length instead of the usual power of the lattice spacing. This behavior is in very good agreement with the theoretical prediction [3].

The theoretical predictions for the continuum values of the LWW-coupling are available in form of nonlinear integral equations [4]. These have to be solved numerically in order to compare with the results obtained from continuum extrapolations on the lattice. The numerical solution is highly non trivial and requires much care. The comparison with Monte Carlo results confirms the predictions very well within statistical errors.

The thesis is structured in the following way: At the beginning (chapter 2) a brief introduction to quantum field theory and the renormalisation group is given. Some peculiarities of the lattice formulation of quantum field theories are explained (finite size effects, lattice artifacts). In chapter 3 the Kosterlitz Thouless theory is reviewed. The correspondence of the XY model to other models is outlined. The numerical methods needed in the simulation of the XY model and the way they were implemented are described in chapter 4. Chapter 5 is dedicated to the exact predictions. The assumptions leading to these results are briefly sketched and a method to solve the nonlinear integral equations is presented. The LWW-coupling plays a central role in the thesis. Chapter 6 describes how it can be used to verify the theoretical predictions. At last the results of the thesis are presented and discussed (chapter 7). Several appendices are devoted to additional calculations, proofs and tables. A short summary in german language is also appended.

Chapter 2

Quantum field theory

The *standard model* of elementary particles describes the smallest constituents of matter and interactions amongst them by means of quantum field theories (QFT). Electromagnetic interactions are described by Feynman's quantum electro dynamics (QED). Weinberg and Salam succeeded in unifying the electromagnetic and weak interactions. The theory of strong interactions is the quantum chromo dynamics (QCD). The interactions have compact, non Abelian gauge groups, $SU(2) \times U(1)$ for the Weinberg Salam model and $SU(3)$ in the QCD.

The standard model has proven to describe the world with a very high accuracy - for example the standard model prediction for the muon anomalous magnetic moment g is ($a_\mu = (g-2)/2$) [5]:

$$a_\mu = (11659177 \pm 7) \times 10^{-10} \tag{2.1}$$

The most precise experimental value is (world average):

$$a_\mu = (11659203 \pm 8) \times 10^{-10} \tag{2.2}$$

In most cases interacting QFTs cannot be solved exactly. Therefore it was necessary to develop approximative methods in order to obtain results that can be compared with experiments. For QED *renormalized perturbation theory* is a very efficient way to calculate transition amplitudes and other physical quantities. In QCD perturbation theory is applicable only in the high energy regime, where the coupling constant α_s is small due to *asymptotic freedom*. At smaller energies α_s becomes large, and perturbation theory fails. Effects like *confinement* can only be studied by non perturbative methods. One widely used method is to discretize the space-time and treat the theory numerically.

It is presumed, that the standard model is a low energy approximation to a theory which unifies gravitation with the other fundamental forces and is suitable to describe the beginning of the universe.

Sometimes it is advantageous to study simpler two dimensional "toy models" instead of a full theory like the QCD. Such models are for example the sine Gordon model or nonlinear σ-models with a global $O(n)$ symmetry. Especially the $n = 3$ model in two space-time dimensions has a lot of properties in common with QCD, e.g. both are asymptotically free and both have instanton solutions. In two dimensions such theories often are *integrable*, i.e. their $S-$matrices and particle spectra are known exactly. Beside the analytical studies also the numerical treatment is less complicated. Usual personal computers can be used for calculations where super computers are needed in the QCD.

2.1 Canonical quantization

Classical field theories may be defined by a Lagrangian density $\mathcal{L}$ from which the Euler-Lagrange equations of motion can be derived via a variational principle. According to Noether's theorem each continuous symmetry of the Lagrangian corresponds to a conservation law of the theory.

For example the Lagrangian of a real scalar field in four dimensional Minkowski space is[1]:

$$\mathcal{L}^{KG} = \frac{1}{2}(\partial_\mu \phi)(\partial^\mu \phi) - \frac{m^2}{2}\phi^2 \tag{2.3}$$

The corresponding equation of motion is the *Klein-Gordon* equation. The canonically conjugated field $\pi(\vec{x}, t)$ is defined by:

$$\pi(\vec{x}, t) = \frac{\partial \mathcal{L}^{KG}}{\partial \dot{\phi}(\vec{x}, t)} \tag{2.4}$$

Two models, formulated on two dimensional Euclidean space-times, that will appear in the following sections are the sine Gordon model with the classical Lagrangian:

$$\mathcal{L}^{sG} = \frac{1}{2}\partial_\mu \phi \partial_\mu \phi + \frac{\alpha}{\beta_{sG}}[1 - \cos(\beta_{sG}\phi)]\,, \tag{2.5}$$

where α and β_{sG} are coupling constants - and the massive Thirring model:

$$\mathcal{L}^{mT} = \bar{\psi}(\not{\partial} + m)\psi - \frac{1}{2} g j_\mu j_\mu\,, \tag{2.6}$$

with

$$j_\mu = \bar{\psi}\gamma_\mu \psi \qquad \text{and} \qquad \not{\partial} = \partial_\mu \gamma_\mu \tag{2.7}$$

The sine Gordon model describes a scalar field with a non linear interaction term. The massive Thirring model describes (two component) fermions with

[1] summation over repeated indices

a four fermion interaction term. The $\gamma-$matrices in two dimensions can be realized with the standard Pauli matrices.

In order to describe many particle systems a quantization of the fields is necessary. The fields are treated as operators that are subject to canonical commutation relations. For scalar fields described by the Lagrangian (2.3) the equal time commutation relations are:

$$\left[\hat{\phi}(\vec{x},t),\hat{\pi}(\vec{x}\,',t)\right] = i\delta(\vec{x}-\vec{x}\,') \tag{2.8}$$

$$\left[\hat{\phi}(\vec{x},t),\hat{\phi}(\vec{x}\,',t)\right] = \left[\hat{\pi}(\vec{x},t),\hat{\pi}(\vec{x}\,',t)\right] = 0 \tag{2.9}$$

Fermions satisfy anti-commutation relations. The dynamics of the quantum field theory is described by Heisenberg's equations of motion.

2.2 Nonlinear $O(n)$ σ-models

Nonlinear σ-models are defined by the classical Lagrangian:

$$\mathcal{L}^{O(n)} = \frac{1}{2g^2}\partial_\mu S^a \partial_\mu S^a, \qquad S^a S^a = 1, \qquad a = 1,2,\ldots,n \tag{2.10}$$

A lot is known about the non Abelian theories with $n \geq 3$. They are asymptotically free [6], i.e their physical couplings approach zero when the energy scale is taken to infinity. Their spectrum consists of an $O(n)$ vector multiplet of massive particles whose scattering is described by a $S-$matrix which is exactly known.

When in the $n = 2$ case the constraint is solved by: $S_1 = \cos\theta$ and $S_2 = \sin\theta$, the Lagrangian (2.10) can be brought into the form

$$\mathcal{L}^{O(n)} = \frac{1}{2g^2}\partial_\mu\theta\partial_\mu\theta\,, \tag{2.11}$$

which is quadratic. Only the angular character of θ distinguishes the $O(2)$ $\sigma-$model from a free theory. In [7] the $O(2)$ model was thoroughly examined. It was suggested that the quantum field theory defined by the massive continuum limit[2] of the XY model coincides with the quantum field theory defined via a formfactor bootstrap method. Strong evidence was given that the $S-$matrix coincides with the $n \to 2$ limit of the $n \geq 3$ models and with the $\beta_{\rm sG} \to \sqrt{8\pi}$ limit of the sine Gordon theory's $S-$matrix. Also the symmetry enhancement that takes place at the level of the S-matrix and the scattering states (the symmetry group being the $SU(2)$) was discussed.

[2]The critical point is approached from the high temperature phase, see chapter 3

2.3 Quantum field theory on a lattice

Feynman's path integral formulation [8] makes the connection between QFTs and statistical systems apparent. The path integral formulated on an Euclidean space-time is equivalent to the partition function of a statistical system.

To be accessible to numerical treatment, the number of degrees of freedom must be made finite. This is usually achieved by introducing a space-time lattice. Such a lattice provides a non perturbative cutoff. UV divergencies are removed and the theory becomes mathematically well defined. After renormalisation the regulator has to be removed, thus physical results are obtained in the continuum limit.

When the action of the $O(2)$ nonlinear σ-model in two dimensions is discretized (lattice spacing a in both directions) in the simplest way, i.e derivatives are replaced by next neighbor differences, the action of the XY model is recovered:

$$\begin{aligned} &\int dx\, dt\ \frac{1}{2g^2}\partial_\mu S^a \partial_\mu S^a \qquad \xleftarrow{a\to 0} \\ &\frac{1}{2g^2}\sum_{x,t}(\vec{s}(x,t)\cdot\vec{s}(x+a,t)+\vec{s}(x,t)\cdot\vec{s}(x,t+a))+\text{const} \end{aligned} \tag{2.12}$$

The XY model is a statistical system which can be thought of as a two dimensional ferromagnet. Its properties are described in chapter 3.1.

2.3.1 The transfer matrix

On a lattice with spatial extent La and temporal extent Ka and periodic boundary conditions in all directions the partition function of the XY model can be written as (spatial and temporal distances are expressed in lattice units):

$$\int \prod_{x=1}^{L}\prod_{t=1}^{K} ds(x,t)\ \exp[-\beta(\vec{s}(x,t)\cdot\vec{s}(x+1,t)+\vec{s}(x,t)\cdot\vec{s}(x,t+1))] \tag{2.13}$$

The integral extends over all possible spin configurations:

$$\int ds = \int_{\mathbb{R}^2} dr^2\ \delta(1-|\vec{r}|) \tag{2.14}$$

With the following definitions

$$Ds(t) := \prod_{x=1}^{L} ds(x,t) \tag{2.15}$$

$$T(t+1,t) := \prod_{x=1}^{L} \exp\left[-\beta\left(\frac{\vec{s}(x,t)\cdot\vec{s}(x+1,t)+\vec{s}(x,t+1)\cdot\vec{s}(x+1,t+1)}{2} + \vec{s}(x,t)\cdot\vec{s}(x,t+1)\right)\right] \tag{2.16}$$

the partition function can be written as:

$$Z = \int \prod_{t=1}^{K} Ds(t)\ T(t+1,t) \tag{2.17}$$

The function T can be regarded as a matrix element of the *transfer matrix* operator:

$$T(t+1,t) = \langle s(t+1)|\hat{T}|s(t)\rangle \tag{2.18}$$

The introduced states are eigenstates of the spin field operator

$$\hat{s}(x)|s(t)\rangle = \vec{s}(x,t)|s(t)\rangle \tag{2.19}$$

They are complete:

$$\int Ds(t)\ |s(t)\rangle\langle s(t)| = \mathbf{1} \tag{2.20}$$

The transfer matrix operator is related to the Euclidean version of the time evolution operator. It can be expressed as an exponential[3] of the Hamilton operator of the theory:

$$\hat{T} = e^{-\hat{H}a}\,, \tag{2.21}$$

Thus, if the transfer matrix $\hat{T}$ of a statistical system is a positive definite operator (which is the case for the XY model), the Hamilton operator of the corresponding quantum theory can be defined by (2.21). The partition function can be expressed in terms of (2.18):

$$\begin{aligned} Z &= \int \prod_{t=1}^{K} Ds(t)\ \langle s(t+1)|\hat{T}|s(t)\rangle \\ &= \int \langle s(K+1)|\hat{T}|s(K)\rangle\ Ds(K)\ \langle s(K)|\hat{T}\ldots|s(1)\rangle\ Ds(1) \\ &= \int Ds(1)\ \langle s(K+1)|\hat{T}^K|s(1)\rangle \\ &= \mathrm{Tr}\ \hat{T}^K \end{aligned} \tag{2.22}$$

[3] In the sense that $e^{-\hat{H}a} = \sum_{n=0}^{\infty} \frac{(-\hat{H}a)^n}{n!}$

The operator identity (2.20) was used many times. The states at $t = 1$ and $t = T+1$ are identified due to periodic boundary conditions. When the trace is evaluated in the eigensystem of the Hamilton operator $\hat{H}|E_i\rangle = E_i|E_i\rangle$ and K is large, the dominating contribution to the partition function comes from the ground state:

$$\text{Tr } \hat{T}^K = \sum_i \langle E_i|e^{-E_i K a}|E_i\rangle \approx e^{-E_0 K a} \tag{2.23}$$

The massgap of the quantum field theory

$$M = E_1 - E_0 \tag{2.24}$$

can also be related to a quantity of the corresponding statistical system. The time slice correlation function is defined by:

$$\begin{aligned} G(t, t+\tau) &= G(\tau) = \langle \vec{S}(t) \cdot \vec{S}(t+\tau)\rangle \\ &= \frac{1}{Z}\int \left(\prod_{t'=1}^{K} Ds(t')\ T(t'+1, t')\right) \vec{S}(t) \cdot \vec{S}(t+\tau) \end{aligned} \tag{2.25}$$

The system has got a translational invariance because of the periodic boundary conditions, therefore the correlation function does not depend on t. The spatially averaged spin fields

$$\vec{S}(t) = \sum_{x=1}^{L} \vec{s}(x, t) \tag{2.26}$$

were introduced. A spatially averaged spin field operator can also be defined:

$$\hat{S}|s(t)\rangle = \sum_{x=1}^{L} \hat{s}(x)|s(t)\rangle = \vec{S}(t)|s(t)\rangle \tag{2.27}$$

The steps in (2.22) can be repeated for the correlation function everywhere except for two time slices:

$$\begin{aligned} G(\tau) &= \frac{1}{Z}\int Ds(1)\ \langle s(1)|\hat{T}^{K-n-\tau}|s(n+\tau)\rangle\ \vec{S}(n+\tau) Ds(n+\tau) \\ &\qquad \langle s(n+\tau)|\hat{T}^{\tau}|s(n)\rangle\ \vec{S}(n) Ds(n)\ \langle s(n)|\hat{T}^{n}|s(1)\rangle \\ &= \frac{1}{Z}\text{Tr } (\hat{T}^{K-n-\tau}\hat{S}\hat{T}^{\tau}\hat{S}\hat{T}^{n}) \end{aligned} \tag{2.28}$$

The trace can be evaluated in the system of energy eigenstates. For large $K - \tau$ the major contribution comes from the ground state.

$$\begin{aligned} G(\tau) &= \frac{\langle E_0|\hat{S}\hat{T}^{\tau}\hat{S}|E_0\rangle e^{-E_0(K-\tau)a}}{e^{-E_0 K a}} \\ &= \sum_i |\langle E_i|\hat{S}|E_0\rangle|^2\ e^{-(E_i - E_0)\tau a} \\ &\underset{\tau \text{ large}}{\approx} |\langle E_1|\hat{S}|E_0\rangle|^2\ e^{-M\tau a} \end{aligned} \tag{2.29}$$

The contribution from $|\langle E_0|\hat{S}|E_0\rangle|^2$ vanishes because the ground state has spin zero. Also contributions from all states with a momentum different from zero vanish, because $\hat{S}$ is a spatially averaged operator. For large arguments the time slice correlation function falls off exponentially. The massgap is related to the correlation length ξ of the system:

$$\xi = \frac{1}{Ma} \tag{2.30}$$

When in the continuum limit $a \to 0$ the massgap is held fixed, the correlation length has to diverge. This happens at critical points of the statistical systems and that is why they play such an important role in lattice quantum field theories.

2.3.2 Finite size techniques

Besides providing an UV cutoff a finite space-time lattice also restricts the theory to a finite volume. When the correlation length of the system is comparable with its spatial extent L, finite size effects become relevant. Present computers are not always capable of dealing with lattices that are large enough to make finite size effects neglible. A solution to the problem is to make explicit use of these effects. This is possible because the strength of finite size effects can serve as a measure of the interactions of the theory. An effective coupling that depends on the size of the system can be defined. This coupling can then be related to more common couplings. For non linear $O(n)\sigma-$models a good choice for a running coupling is the *LWW-coupling* [2]:

$$\bar{g}^2(L) = \frac{2M(L)L}{n-1} \tag{2.31}$$

It depends on the finite volume massgap of the theory. The scaling of the coupling is described by its $\beta-$function:

$$\beta(\bar{g}^2) = -L\frac{\partial \bar{g}^2}{\partial L} \tag{2.32}$$

For $n > 2$ this function can be calculated perturbatively:

$$\beta(u) \underset{u\to 0}{\approx} -u^2 \sum_{l=0}^{\infty} b_l u^l \tag{2.33}$$

More suitable for lattice simulations is the *step scaling function*. It describes how the coupling changes when L is scaled by a factor s:

$$\sigma(s, \bar{g}^2(L)) = \bar{g}^2(sL) \tag{2.34}$$

It is related to the $\beta-$function by:

$$\ln s = -\int_u^{\sigma(s,u)} dv\ \frac{1}{\beta(v)} \tag{2.35}$$

The step scaling function can be calculated numerically (section 6.2) on relatively small lattices. When it is known, the high energy properties of the theory can be linked with the low energy properties.

2.3.3 Lattice artifacts

The lattice regularisation is equivalent to a momentum cut off $\Lambda_{\text{cut}} \propto \frac{1}{a}$ that has to be removed after renormalisation. Numerical calculations can only be done on finite lattices and thus only a restricted range of lattice spacings a is accessible. Therefore knowledge of the functional form of the *lattice artifacts* is essential for a reliable extrapolation to the continuum. Symanzik has shown that in non Abelian bosonic theories the leading lattice artifacts decrease as $\mathcal{O}(a^2(\ln(a))^{l+1})$ in each order of perturbation theory [9] [10]. It is assumed that this behavior holds beyond perturbation theory and extrapolations are usually done assuming a decrease of lattice artifacts roughly proportional to a^2.

Recent numerical studies [11] show that in the $O(3)$ nonlinear $\sigma-$model lattice artifacts are better described by an ansatz linear in a. This discrepancy is subject to current research.

For the Abelian $O(2)$ model the continuum is approached more slowly than $\mathcal{O}(a^2)$ or even $\mathcal{O}(a)$. J. Balog has derived an *inverse logarithmic* approach to the continuum [3] that follows from Kosterlitz Thouless theory (see chapter 3). He showed that leading lattice artifacts are universal and calculable for a certain class of lattice actions and observables. In [7] this behavior was confirmed by numerical simulations of the two point function of the Noether current. One of the main goals of this thesis is to check whether Balog's prediction holds for the step scaling function (2.34).

2.4 RG transformations

Quantum field theories are recovered at critical points of statistical systems. The physics at these points is very interesting. Near such continuous phase transitions the correlation length grows very large and becomes the only relevant scale of the system. Many properties of such a system loose their dependence on its microscopic details and instead exhibit *universal behavior*. One way to find out more about the critical behavior of a given system (e.g. calculate its critical exponents) is a renormalisation group (RG) study. As one is interested in the large scale physics of the systems (because ξ is large), one can apply a transformation, in the course of which short range degrees of freedom are integrated out - the system is considered at a larger scale L. Such a transformation can for example be a *block spin* transformation or a continuous scale transformation like in section 3.3. After the transformation the partition function of the system is brought into its original functional form. To achieve this the couplings of the theory have to be redefined. From

this procedure a set of RG equations is obtained whose solutions describe the flow of the couplings when the scale is changed. Exactly at a critical point the correlation length diverges and the system is *scale invariant*. These points correspond to fixed points of the RG flow.

Quantities that are invariant under such scaling transformations are called universal. They have a constant value along a RG trajectory.

During a RG transformation new coupling constants can occur. Block spin transformations can for example connect diagonal neighbors with each other. The RG transformation $\mathcal{R}$ acts on the space of all possible couplings $\{K\}$:

$$\mathcal{R}(\{K\}) = \{K'\} \tag{2.36}$$

Assuming that a fixed point exists at $\{K^*\}$ and that $\mathcal{R}$ is differentiable around this fixed point makes it possible to write down a linearized version of the RG equations [12]:

$$K'_a - K^*_a = \sum_b J_{ab}(K_b - K^*_b) + \mathcal{O}((K - K^*)^2) \tag{2.37}$$

The matrix **J** is defined by:

$$J_{ab} = \left.\frac{\partial K'_a}{\partial K_b}\right|_{K=K^*} \tag{2.38}$$

When its right eigenvectors are ϕ^i and the corresponding eigenvalues λ^i, *scaling variables* may be introduced

$$u_i := \sum_a \phi^i_a (K_a - K^*_a)\,, \tag{2.39}$$

whose transformation (near the fixed point) is given by (no summation):

$$u'_i = \lambda^i u_i \tag{2.40}$$

The scaling variables can be categorized in terms of quantities y_i defined by $\lambda^i = s^{y_i}$, where s is the factor by which the scale is changed during the transformation:

$y_i > 0$: u_i is a *relevant* scaling variable, it is driven away from its fixed point value when the RG transformation is repeated.

$y_i < 0$: u_i is an *irrelevant* scaling variable. It vanishes when the transformation is repeated.

$y_i = 0$: u_i is a *marginal* scaling variable. Its behavior cannot be extracted from the linearized version of the RG equations.

If in the XY model next to the nearest neighbors interactions were introduced, the corresponding scaling variable would be irrelevant. The long range behavior of this system and the original XY model near their critical points would be the same. Universal properties can be derived from the scaling variables. Although the XY model has got only one coupling constant, it can be shown (section 3.3) that it has got two relevant scaling variables.

2.5 Critical exponents

Near continuous phase transitions various thermodynamic quantities of statistical systems obey power laws. When the deviation from the critical point of a magnet is parametrized by the reduced temperature $t = \frac{T_c - T}{T_c}$ and the reduced external field $h = \frac{H}{k_B T_c}$ critical indices can be defined as follows (e.g. [12]):

α: Specific heat: $C \propto |t|^{-\alpha}$.

β: Spontaneous magnetization: $\lim_{H \to 0^+} \propto (-t)^{\beta}$.

γ: Zero field susceptibility: $\chi \propto |t|^{-\gamma}$.

δ: Magnetization at $t = 0$: $M \propto |h|^{1/\delta}$.

ν: Correlation length: $\xi \propto |t|^{-\nu}$.

η: Correlation function at the critical point: $g(r) \propto 1/r^{d-2+\eta}$.

z: The typical relaxation time: $\tau \propto \xi^z$.

These exponents are universal. They have exactly the same values for all systems in the same universality class. To which class a system belongs depends mostly on its symmetries and the dimensionality of space. For example three dimensional, uniaxial ferromagnets have the same critical exponents as simple fluids.

Chapter 3

Kosterlitz Thouless theory

3.1 The XY model

In the past much effort was made to explore the statistical properties of the XY model. In this section I will sum up some of the most interesting results that were obtained.

3.1.1 Definition of the model

On each site i of a two dimensional lattice, there is a classical spin $\vec{s}_i$ with two components. Neighboring spins do interact with each other. If the size of the system is finite ($L \times K$), then boundary conditions must be declared. Usually, periodic boundary conditions in both directions are applied, but different choices (e.g. free boundary conditions) are possible as well. The energy of the system is:

$$H = -\beta \sum_{\langle l,k \rangle} \vec{s}_l \cdot \vec{s}_k \tag{3.1}$$

The sum is performed over all neighbors on the lattice. Each spin has unit length:

$$\vec{s}_i \cdot \vec{s}_i = 1 \tag{3.2}$$

This constraint can be solved with:

$$\vec{s}_i = \begin{pmatrix} \cos\theta_i \\ \sin\theta_i \end{pmatrix} \tag{3.3}$$

Then the energy reads:

$$H = -\beta \sum_{\langle l,k \rangle} \cos(\theta_l - \theta_k) \tag{3.4}$$

The energy is O(2)-symmetric, i.e. a rotation of all spins by the same angle, does not change the system's energy. The angular character of the variables

θ will play a great role in explaining the special phase transition that occurs in the model (section 3.1.3).

The system's partition function is:

$$Z = \int D\theta \ \exp\left[\beta \sum_{\langle l,k \rangle} \cos(\theta_l - \theta_k)\right] \tag{3.5}$$

Here, the Boltzmann factor $1/(k_B T)$ was incorporated into the coupling constant. One integrates over all possible configurations:

$$\int D\theta = \prod_n \int_{-\pi}^{\pi} d\theta_n \tag{3.6}$$

A physical observable A has got the expectation value:

$$\langle A \rangle = \frac{1}{Z} \int D\theta \ A(\theta) \exp\left[\beta \sum_{\langle l,k \rangle} \cos(\theta_l - \theta_k)\right] \tag{3.7}$$

Common observables are for example the magnetization:

$$\vec{M} = \langle \vec{s}_i \rangle = \frac{1}{Z} \int D\theta \begin{pmatrix} \cos\theta_i \\ \sin\theta_i \end{pmatrix} \exp\left[\beta \sum_{\langle l,k \rangle} \cos(\theta_l - \theta_k)\right] \tag{3.8}$$

or the spin-spin correlation function:

$$g(\vec{r}_x) = \langle \vec{s}_0 \cdot \vec{s}_x \rangle = \frac{1}{Z} \int D\theta \ \cos(\theta_0 - \theta_x) \exp\left[\beta \sum_{\langle l,k \rangle} \cos(\theta_l - \theta_k)\right] \tag{3.9}$$

Where $\vec{r}_x$ denotes the position of lattice point x.

3.1.2 The Gaussian approximation and spin-waves

At low temperatures (large β) one expects neighboring spins to point into similar directions. Then the cosine in (3.4) can be expanded and all orders higher then two may be neglected. This leads to the spin-wave approximation of the XY model [13]:

$$H = -\beta \sum_{\langle l,k \rangle} \left(1 - \frac{(\theta_l - \theta_k)^2}{2}\right) \tag{3.10}$$

The constant part cancels out when expectation values are calculated, so the partition function may be written as:

$$Z_{SW} = \int D\theta \ \exp\left[-\frac{\beta}{2}\sum_{\langle l,k\rangle}(\theta_l-\theta_k)^2\right] \tag{3.11}$$

$$Z_{SW} = \int D\theta \ \exp\left[-\frac{\beta}{2}\sum_{l,k}\theta_l M_{lk}\theta_k\right] \tag{3.12}$$

The matrix M is nearly[1] triagonal:

$$M_{lk} = \begin{cases} 4 & \text{if } l=k \\ -2 & \text{if } l \text{ and } k \text{ are neighbors} \end{cases} \tag{3.13}$$

If the integral boundaries are extended to infinity, which is a good approximation for large β

$$\prod_n \int_{-\pi}^{\pi} d\theta_n \to \prod_n \int_{-\infty}^{\infty} d\theta_n \,, \tag{3.14}$$

integral (3.12) becomes Gaussian and correlation functions can be calculated with help of the generating functional [14]:

$$\left\langle \exp\left[i\sum_{j=1}^{m} q_j\theta_j\right]\right\rangle = \exp\left[-\frac{2}{\beta}\sum_{j,k} q_j q_k G(\vec{r}_j-\vec{r}_k)\right] \tag{3.15}$$

The lattice Green function in two dimensions is:

$$G(\vec{r}) = \int_{-\pi}^{\pi} \frac{d\vec{k}}{(2\pi)^2} \frac{e^{i\vec{k}\cdot\vec{r}}}{\sum_{a=1}^{2} 4(1-\cos k_a)} \tag{3.16}$$

From eq. (3.15) the magnetization (x-component) can be obtained directly:

$$M_x = \langle\cos(\theta_k)\rangle = \mathrm{Re}\langle e^{i\theta_k}\rangle = \mathrm{Re}\exp\left[-\frac{2G(0)}{\beta}\right] \tag{3.17}$$

The integral in (3.16) is divergent. $G(0)$ becomes infinite and the magnetization is zero. This behavior is in accordance with the Mermin-Wagner-theorem [15], which states that global symmetries do not break spontaneously in one and two dimensional systems with short range interactions. That means that the magnetization remains zero for any value of the coupling. In higher dimensions the corresponding lattice Green function is not divergent, and there may be a magnetized phase at low temperatures.

[1] Due to periodic boundary conditions there are to entries which do not lie on the triagonal.

Eq. (3.15) enables us also to calculate the spin-spin correlation function:

$$\begin{aligned} g(\vec{r}_x) &= \mathrm{Re}\langle e^{i\theta_0} e^{-i\theta_x} \rangle \\ &= \mathrm{Re}\ e^{-\frac{G(0)-G(\vec{r}_x)}{\beta}} \\ &= \mathrm{Re}\ e^{\frac{\Gamma(\vec{r}_x)}{\beta}} \end{aligned} \tag{3.18}$$

$\Gamma(\vec{r}_x)$ is finite because the infinities in $G(0)$ and $G(\vec{r}_x)$ cancel each other. For large separations Γ is nearly isotropic and an excellent approximation [16] is given by:

$$\Gamma(r) \approx \frac{1}{2\pi} \ln \frac{r}{r_0} \tag{3.19}$$

The constant is:

$$r_0 = a \frac{e^{-\gamma}}{2\sqrt{2}} \tag{3.20}$$

where γ denotes Euler's constant and a is the lattice spacing. Now the correlation function at large separations can be written as:

$$g(|\vec{r}_x|) \approx \left| \frac{\vec{r}_x}{r_0} \right|^{\frac{1}{2\pi\beta}} \tag{3.21}$$

The correlations decay according to a power law, which is typical for systems near their critical points. The difference is that here the critical index is neither constant nor universal but varies with temperature. The XY model remains critical in its whole low temperature phase.

3.1.3 The Kosterlitz-Thouless phase transition

At high temperatures (small β) the exponential in the partition function can be expanded in β and higher order terms may be neglected. In the following it is assumed that $\vec{r}_0$ and $\vec{r}_n$ are on the same axis and the separation between

them in lattice units is n. The correlation function is:

$$\begin{aligned} g(|\vec{r}_0 - \vec{r}_n|) &= \mathrm{Re}\langle e^{i\theta_0} e^{-i\theta_n} \rangle \\ &= \mathrm{Re}\frac{1}{Z}\int D\theta \; e^{i(\theta_0-\theta_n)} \prod_{\langle k,l\rangle} \sum_{j=0}^{\infty} \frac{\beta^j}{j!} e^{ij(\theta_k-\theta_l)} \\ &= \mathrm{Re}\frac{1}{Z}\int D\theta \; e^{i[(\theta_0-\theta_1)+(\theta_1-\theta_2)+\ldots+(\theta_{n-1}-\theta_n)]} \\ &\quad \times \Big(1 + \sum_{\langle k,l\rangle} \beta e^{i(\theta_k-\theta_l)} \\ &\quad + \sum_{\langle k,l\rangle} \sum_{\langle k',l'\rangle} \beta^2 e^{i[(\theta_k-\theta_l)+(\theta_{k'}-\theta_{l'})]} \\ &\quad + \sum_{\langle k,l\rangle} \frac{\beta^2}{2} e^{2i(\theta_k-\theta_l)} \\ &\quad + \sum_{\langle k,l\rangle} \sum_{\langle k',l'\rangle} \frac{\beta^3}{2} e^{i[(\theta_k-\theta_l)+2(\theta_{k'}-\theta_{l'})]} + \ldots\Big) \end{aligned} \tag{3.22}$$

As

$$\int_{-\pi}^{+\pi} d\theta \; e^{i\theta} = 0 \quad \text{and} \quad \int_{-\pi}^{+\pi} d\theta \; 1 = 2\pi, \tag{3.23}$$

only terms where the phases add to zero will contribute. The first term where this happens is of order β^n. The correlation function is nearly isotropic for large separations, therefore the results can be generalized to arbitrary $|\vec{r}_0 - \vec{r}_n| \approx n$. The correlation function in leading order is:

$$g(|\vec{r}|) \propto 2\pi\beta^{|\vec{r}|} = e^{\ln(2\pi\beta)|\vec{r}|} \tag{3.24}$$

The logarithm is negative for small β, so the correlations decay exponentially. This is a typical high temperature behavior that can be observed in many systems.

The preceding considerations indicate that there is a temperature where a phase transition occurs. This critical temperature separates a phase with infinite correlation length and spin-waves, from a phase with fast decaying correlations and finite correlation length, where the Gaussian approximation fails. An explanation for this phase transition was given by J.M. Kosterlitz and D.J. Thouless [1] [17]. They argued that above a critical temperature *vortex*-configurations (fig. 3.1) become very important. The Gaussian approximation does not preserve the angular character of θ, therefore it cannot describe vortices.

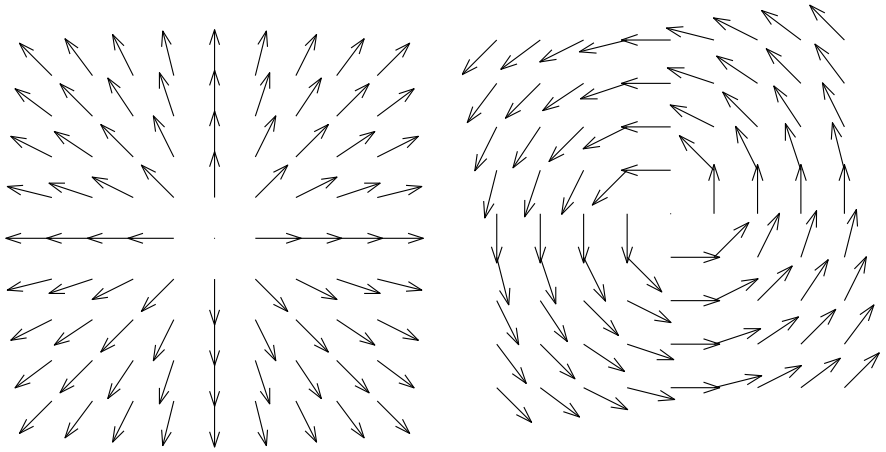

Figure 3.1: Vortex-configurations. The left one is obtained from the right one by a global O(2)-transformation.

In a vortex, the angle between two neighboring spins is approximately $1/r$, where r is the distance from the center. To give an estimate for the energy of an isolated vortex, one can use eq. (3.10). Replacing the sums by integrals leads to:

$$E_{\text{Vortex}} \approx \frac{\beta}{2} \int_{-\pi}^{+\pi} d\phi \int_{a}^{R} dr \; r \left(\frac{1}{r}\right)^2 = \pi\beta \ln\left(\frac{R}{a}\right) \tag{3.25}$$

The energy diverges when a thermodynamic limit is taken. Nevertheless the occurrence of vortices becomes plausible when the free energy $F = E - ST$ is considered. A vortex is specified completely by the position of its center, so in a system of size $(R/a)^2$, its entropy is:

$$S_{\text{Vortex}} = 2k_B \ln\left(\frac{R}{a}\right) \tag{3.26}$$

The free energy

$$F_{\text{Vortex}} = (\pi\beta - 2k_B T) \ln\left(\frac{R}{a}\right) \tag{3.27}$$

changes its sign at a certain temperature. Below this temperature the occurrence of isolated vortices is very unlikely. Above this temperature they play an important role. This phenomenon is often called *vortex-condensation*.

3.2 The Villain model

Many useful considerations can be done with help of the Villain model [18]. It preserves the symmetries of the original model and is accessible to exact calculations due to its Gaussian structure. The Villain model exhibits the same critical behavior as the XY model [19]. For small temperatures it is a good approximation to the XY model. Vortex and spin-wave degrees of freedom decouple from each other in the Villain model.

The partition function of the Gaussian approximation to the XY model is:

$$Z_{SW} = \int D\theta \prod_{\langle l,k \rangle} z(\theta_l - \theta_k) \tag{3.28}$$

with

$$z(\theta) = \exp\left[-\frac{\beta}{2}\theta^2\right]. \tag{3.29}$$

One possibility to make $z(\theta)$ 2π-periodic is to periodically repeat its structure:

$$z_V(\theta) = \sum_{m=-\infty}^{+\infty} \exp\left[-\frac{\beta}{2}(\theta - 2\pi m)^2\right] \tag{3.30}$$

$$= (2\pi\beta)^{-\frac{1}{2}} \sum_{n=-\infty}^{+\infty} \exp\left[in\theta - \frac{n^2}{2\beta}\right] \tag{3.31}$$

The equivalence between (3.30) and (3.31) is shown in appendix A.1. With a little change of notation and omitting the factor $(2\pi\beta)^{\frac{1}{2}}$ the partition function of the Villain model is written as (no summation over repeated indices):

$$Z_V = \int D\theta \prod_{\vec{x},\mu} \sum_{n_\mu(\vec{x})=-\infty}^{+\infty} \exp\left(-\frac{n_\mu^2(\vec{x})}{2\beta} + i n_\mu \partial_\mu \theta(\vec{x})\right) \tag{3.32}$$

$\theta(\vec{x})$ is the angle of a spin on the lattice site $\vec{x}$, μ is a direction on the lattice and ∂_μ is the difference operator: $\partial_\mu\theta(\vec{x}) = \theta(\vec{x} + \vec{a}_\mu) - \theta(\vec{x})$. Each link has its own summation variable $n_\mu(\vec{x})$.

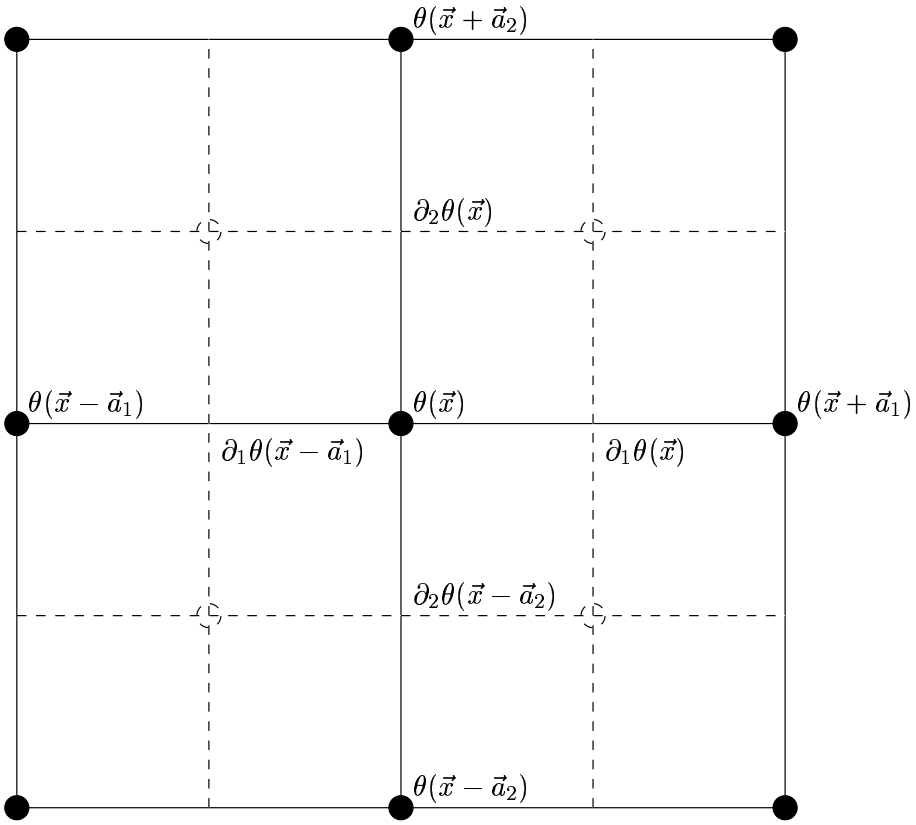

Figure 3.2: Lattice point $\vec{x}$ and its neighbors

For each integral $\int d\theta(\vec{x})$ there are only four terms that contain $\theta(\vec{x})$ (fig. 3.2):

$$\partial_1\theta(\vec{x}), \qquad \partial_2\theta(\vec{x}), \tag{3.33}$$

$$\partial_1\theta(\vec{x}-\vec{a}_1) \quad \text{and} \quad \partial_2\theta(\vec{x}-\vec{a}_2) \tag{3.34}$$

The appropriate factor in (3.32) is:

$$\sum_{n_1(\vec{x})}\sum_{n_1(\vec{x}-\vec{a}_1)}\sum_{n_2(\vec{x})}\sum_{n_2(\vec{x}-\vec{a}_2)} \exp\big[in_1\partial_1\theta(\vec{x}) + in_2\partial_2\theta(\vec{x}) - in_1\partial_1\theta(\vec{x}-\vec{a}_1) - in_2\partial_2\theta(\vec{x}-\vec{a}_2)\big] \tag{3.35}$$

The associated integral differs from zero only if the phases cancel each other. Contributing terms obey the condition:

$$n_1(\vec{x}) + n_2(\vec{x}) - n_1(\vec{x}-\vec{a}_1) - n_2(\vec{x}-\vec{a}_2) \; = \sum_\mu \partial_\mu n_\mu(\vec{x}) = 0 \tag{3.36}$$

The discrete divergence of $\vec{n}(\vec{x})$ is zero, therefore $\vec{n}$ can be written as a "curl"

of a scalar, integer valued field $m(\vec{x})$:

$$n_\mu(\vec{x}) = \sum_\nu \epsilon_{\mu\nu}\partial_\nu m(\vec{x}) \tag{3.37}$$

And, dropping a constant factor, the partition function finally becomes:

$$\begin{aligned} Z_V &= \prod_{\vec{x},\mu} \sum_{m(\vec{x})=-\infty}^{+\infty} \exp\left[-\frac{1}{2\beta}(\partial_\mu m(\vec{x}))^2\right] \\ &= \sum_{\{m(\vec{x})\}=-\infty}^{+\infty} \exp\left[-\frac{1}{2\beta}\sum_{\vec{x},\mu}(\partial_\mu m(\vec{x})^2)\right], \end{aligned} \tag{3.38}$$

The sum in the last line is a sum over all possible configurations. This duality transformation replaced the periodic variables θ by discrete integers m, which are located on the dual lattice (dashed lines in fig. 3.2). The partition function (3.38) is essentially the same as that of a solid-on-solid model (SOS) [20]. These models describe the surfaces of crystals. The value of $m(\vec{x})$ is the deviation of the plaquette $\vec{x}$ from a planar surface ($m = 0$). At small β, the surface is smooth. At a critical temperature a roughening transition takes place, and the surface becomes rough, i.e. distant points have uncorrelated heights.

Poisson's summation formula

$$\sum_{m=-\infty}^{+\infty} f(m) = \sum_{q=-\infty}^{+\infty} \int_{-\infty}^{+\infty} d\phi\ f(\phi)e^{i2\pi q\phi} \tag{3.39}$$

can be applied to eq. (3.38). The results is:

$$Z_V = \int D\phi \sum_{\{q(\vec{x})\}=-\infty}^{+\infty} \exp\left[-\frac{1}{2\beta}\sum_{\vec{x},\mu}(\partial_\mu\phi(\vec{x}))^2 + i2\pi\sum_{\vec{x}} q(\vec{x})\phi(\vec{x})\right] \tag{3.40}$$

When the integration over ϕ is carried out, the partition function factorizes into a spin-wave part and a Coulomb-gas part:

$$Z_V = Z_{SW}\, Z_{CG} \tag{3.41}$$

with

$$Z_{CG} = \sum_{\{q(\vec{x})\}=-\infty}^{+\infty} \exp\left[-2\pi^2\beta\sum_{\vec{x},\vec{z}} q(\vec{x})G(\vec{x}-\vec{z})q(\vec{z})\right] \tag{3.42}$$

When the infinite part of G is split up ($G(\vec{x}) = G(0) + \Gamma(\vec{x})$) it becomes apparent that only configurations with $\sum_{\vec{x}} q(\vec{x}) = 0$ survive the continuum

limit. Approximating $\Gamma(\vec{x})$ by its long range behavior leads to the final form of the partition function:

$$Z_{CG} = \sum_{\{q(\vec{x})\}}{}' \exp\left(\pi\beta \sum_{\vec{x}\neq\vec{z}} q(\vec{x}) \ln\left|\frac{\vec{x}-\vec{z}}{a}\right| - \ln y \sum_{\vec{x}} q^2(\vec{x})\right) \tag{3.43}$$

The summation $\sum'$ is performed over all configurations which satisfy the neutrality condition $\sum_{\vec{x}} q(\vec{x}) = 0$ and $y = \exp(-\pi^2\beta/2)$ denotes the *chemical activity*.

Vortices and spin-waves do not interact with each other in the Villain model. The vortices behave like charged particles in two dimensions. Their vorticity q corresponds to the charge. The interaction is logarithmic.

3.3 The renormalization group calculation

The calculation is carried out on the Villain model, the results are universal and thus also valid for the XY model. For small y the most important configurations in (3.43) are those with zero vortices and those with a vortex anti-vortex pair (It was shown in context of the sine Gordon model that higher-than-one charges are irrelevant [21]). When all other configurations are neglected, the continuum version of (3.43) takes the form:

$$1 + \frac{y^2}{a^4} \iint\limits_{|\vec{x}-\vec{z}|>a} d^2x\, d^2z \left|\frac{a}{\vec{x}-\vec{z}}\right|^{2\pi\beta} \tag{3.44}$$

The distance between the vortices cannot be less then a. The RG transformation changes this cutoff: $a \to \lambda a$. After the transformation the partition function can be brought into it's original functional form (approximatively) when the couplings β and y depend on λ and transform according to the following RG-equations:

$$\frac{d}{d\lambda}\frac{1}{\beta} = \frac{\pi^3 y}{\lambda} \tag{3.45}$$

$$\frac{d}{d\lambda} y = \frac{2-\pi\beta}{\lambda} y \tag{3.46}$$

This equations define a RG-flow (fig. 3.3). They are valid for $y \to 0$. Higher order RG-equations were derived by Amit et. al. [21].

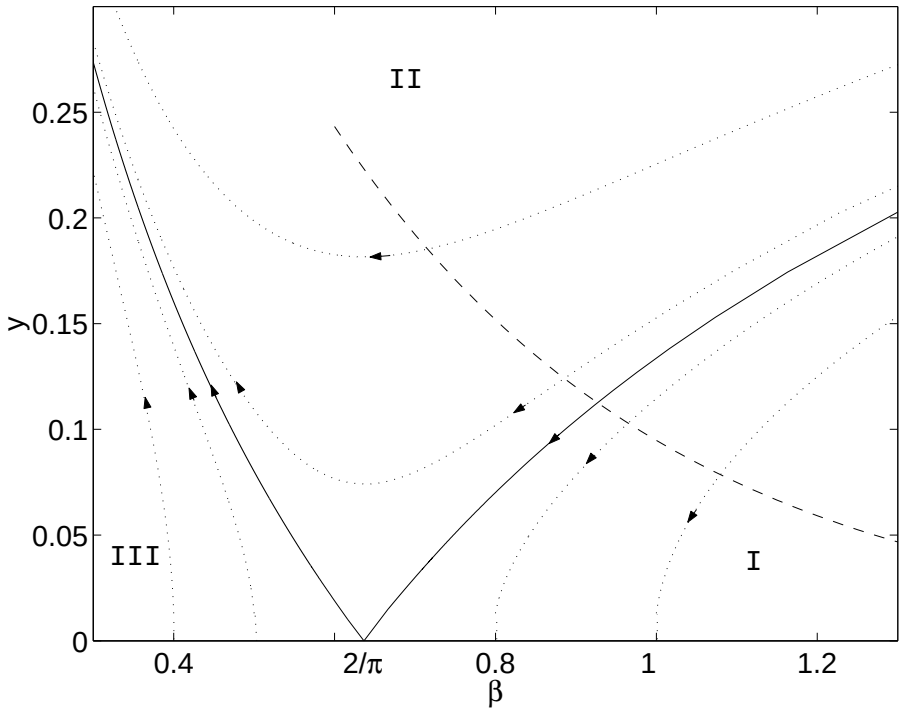

Figure 3.3: The RG flow of a Kosterlitz Thouless fixed point. The dashed line is non universal and characterizes the Villain model.

The dashed line corresponds to the Villain model with $y = \exp(-\pi^2\beta/2)$. The XY model with standard action is characterized by a different non universal line, which crosses the critical surface (the trajectory that ends in $\beta = 2\pi$, $y = 0$) at $\beta \approx 1.1197$. The long range behavior of all points in region I is governed by the line of fixed points at $\beta > 2/\pi, \quad y = 0$. This behavior is that of a system with spin-waves only ($y = 0$). In this region vortices occur in bound pairs. In the language of the Coulomb gas the system contains only neutral molecules and behaves like an insulator. In region II free vortices can appear, the Coulomb gas becomes a plasma (the surface of the crystal becomes smooth).

From the RG-equations the critical exponents (defined in section 2.5) of the XY model can be derived. The phase transition is of infinite order (i.e. the free energy and all its derivatives are smooth at β_c), therefore not all the exponents typical for second order phase transitions can be defined. Instead of obeying the usual power law behavior the correlation length diverges according to

$$\xi \approx A \exp\left[\frac{B}{\sqrt{\beta_c - \beta}}\right] \tag{3.47}$$

when the critical point is approached from the vortex phase and stays infinite in the spin-wave phase. A and B are non universal constants. The other

exponents can be defined when they are expressed in terms of the correlation length:

$$C \propto \quad \xi^{\alpha} \qquad \alpha = -2 \tag{3.48}$$

$$\chi \propto \quad \xi^{\gamma} \qquad \gamma = 15 \tag{3.49}$$

$$g(r) \propto \quad 1/r^{\eta} \qquad \eta = \frac{1}{4} \tag{3.50}$$

$$M \propto \quad |h|^{1/\delta} \qquad \delta = 15 \tag{3.51}$$

In addition to the systems discussed in this section, a Kosterlitz Thouless phase transition also occurs in the sine Gordon model [22] [23], in the massive Thirring model [24], in 2d He^4 films [25] [26] and in many other systems. All these systems are suitable to study the critical properties of the XY model.

Chapter 4

Monte Carlo

4.1 General

Monte Carlo simulation is a method to obtain approximate values for averages over statistical ensembles. In most cases the number of possible configurations that a system can adopt is very high, actually it is even infinite in case of the XY model. This makes an evaluation of the partition function and the calculation of averages with standard numerical integration methods impossible. The idea behind Monte Carlo simulations is to create a finite number of representative configurations. *Simple sampling* methods create each configuration with the same probability. The disadvantage is that most terms are suppressed by a very small Boltzmann factor in the calculation of averages. To avoid this, *importance sampling* is implemented where the created configurations already have the desired distribution [1]. If n independent configurations were created, a Monte Carlo estimate for the observable A (in thermodynamic equilibrium) would be:

$$\langle A \rangle_{\mathrm{MC}} = \frac{1}{n} \sum_{i=1}^{n} A_i \tag{4.1}$$

A_i is the value of the observable evaluated on the i_{th} configuration. For large n $\langle A \rangle_{\mathrm{MC}}$ is a good estimate for the exact mean $\langle A \rangle$

The task of a Monte Carlo algorithm is to create configurations $\{S_i\}$ that are independent and are distributed according to the probability density function

$$P(S_i) = \frac{1}{Z} \exp\left(-\frac{1}{k_B T} H(S_i) \right) , \tag{4.2}$$

where $H(S_i)$ is the energy of the system in the configuration S_i.

In most cases such *independent sampling* is not practicable. Instead most algorithms generate a *Markov chain* of configurations: A configuration S_i is

[1] Only importance sampling algorithms are considered from now on

obtained randomly from its preceding configuration S_{i-1}. If the transition probability $W(S \to S')$ is chosen properly then after a number of iterations configurations distributed according to (4.2) are obtained from arbitrary starts. These are not fully independent, which complicates the calculation of statistical errors.

The transition probability, has the properties

$$W(S \to S') \geq 0, \qquad \sum_{S'} W(S \to S') = 1 \tag{4.3}$$

In order to obtain a valid Monte Carlo algorithm $W(S \to S')$ has to obey two additional conditions:

1. Stability:
$$\sum_{S} P(S)W(S \to S') = P(S') \tag{4.4}$$

2. Ergodicity: $\exists n$ such that
$$W^n(S \to S') > 0 \tag{4.5}$$
for arbitrary S and S'.

It can be shown, that if these two conditions are fulfilled every starting configuration will lead (after sufficiently many steps) to configurations that have the desired distribution. This process is called *equilibration*. Before measurements can start the system must be brought to equilibrium, which may take more or less time, depending on the algorithm and the considered problem.

Instead of proving stability directly it is sufficient to show that an algorithm satisfies *detailed balance*:

$$P(S)W(S \to S') = P(S')W(S' \to S) \tag{4.6}$$

If (4.6) holds, (4.4) will be fulfilled automatically.

4.2 Statistical errors of primary quantities

Before turning to special realizations of Monte Carlo algorithms, I want to discuss shortly how statistical errors are calculated. If all configurations were independent, the statistical error of a primary quantity (i.e. a quantity that is obtained directly from the Monte Carlo experiment) calculated according to (4.1) would be:

$$\delta A = \sqrt{\frac{\sigma_A^2}{n}}\,, \tag{4.7}$$

where $\sigma_A^2 = \langle A \rangle_{\mathrm{MC}}^2 - \langle A^2 \rangle_{\mathrm{MC}}$ is the variance. However as two subsequent configurations are correlated with each other the calculation becomes more involved. The *autocorrelation function* is defined as:

$$\Gamma_A(t) = \langle A_s A_{s+t} \rangle - \langle A \rangle^2 \tag{4.8}$$

It does not depend on s (provided that the system is equilibrated). For large t autocorrelations decay exponentially:

$$\Gamma_A(t) \propto \exp\left(-\frac{t}{\tau_A}\right) \tag{4.9}$$

The exponential autocorrelation time τ_A is a measure for the magnitude of correlations. Taking into account the correlation between subsequent measurements, the statistical error can be calculated according to:

$$\delta A = \sqrt{\frac{2\tau_{\mathrm{int},A}\ \sigma_A^2}{n}} \tag{4.10}$$

where $\tau_{\mathrm{int},A}$ is the integrated autocorrelation time:

$$\tau_{\mathrm{int},A} = \frac{1}{2} + \sum_{t=1}^{+\infty} \frac{\Gamma_A(t)}{\sigma_A^2} \tag{4.11}$$

Usually the sum is truncated, when the contribution of the remaining terms is believed to be smaller than their statistical errors.

4.3 Statistical errors of derived quantities

Often quantities F are obtained from a primary quantity by

$$F = f(\langle A \rangle). \tag{4.12}$$

An estimate for this derived quantity is $F \approx f(\langle A \rangle_{\mathrm{MC}})$, but if f is a nonlinear function the calculation of the statistical error (taking into account the autocorrelations) gets involved. Simple methods to estimate the error are *Jackknife* and *Binning*.

4.3.1 Binning

The idea behind binnig is to divide the available A_i into N_b bins of size B. For each bin b the value of F can be calculated:

$$F_{b,B} = f\left(\frac{1}{B} \sum_{i=1+(b-1)B}^{bB} A_i\right) \tag{4.13}$$

If the bins are large enough (much bigger then the integrated autocorrelation time) the resulting $F_{b,B}$ are almost uncorrelated, because correlations between the bins occur only at their boundaries and can be neglected. The statistical error is according to (4.7):

$$\delta F = \sqrt{\frac{\sum_{b=1}^{N_B} \left(F_{b,B} - \frac{1}{N_B} \sum_{b'=1}^{N_B} F_{b',B} \right)^2}{N_B(N_B-1)}} \tag{4.14}$$

4.3.2 Jackknife

Binning requires a large amount of data to work, especially when the autocorrelation times are big. A similar method where this problem is less severe is jackknife. Again N_B averages are calculated, but this time the bins have the size $(N_B-1)B$:

$$F_{b,\bar{B}} = f\left(\frac{1}{(N_B-1)B} \left(\sum_{i=1}^{(b-1)B} A_i + \sum_{i=bB+1}^{N_B B} A_i \right) \right) \tag{4.15}$$

Taking into account that the $F_{b,\bar{B}}$ are not independent, the error can be approximated by:

$$\delta F = \sqrt{\frac{N_B-1}{N_B} \sum_{b=1}^{N_B} \left(F_{b,\bar{B}} - \frac{1}{N_B} \sum_{b'=1}^{N_B} F_{b',B} \right)^2} \tag{4.16}$$

4.4 Critical slowing down

As discussed in section 2.5, near continuous phase transitions physical quantities often exhibit power law behaviors, where the exponents are universal. Generally the correlation length ξ diverges and the system shows correlations over long distances. Then it is very difficult to create Monte Carlo configurations that are independent. Near a critical point (large ξ) the autocorrelation time diverges as

$$\tau \approx c\xi^z. \tag{4.17}$$

when ξ is much smaller[2] than L. The dynamical critical exponent z depends on the chosen algorithm. For algorithms with local updating (local means that in an elementary update only one site of the lattice is changed) like Metropolis this exponent is $z \approx 2$, which makes an efficient simulation of the system near its phase transition impossible. Over-relaxation algorithms [27] have $z \approx 1$ which still is problematic.

[2] When ξ is not much smaller than L, the autocorrelation time diverges as $\tau \approx f(L/\xi)L^z$

The solution to the problem are algorithms where updates happen on all scales. Prominent examples are multi-grid algorithms and cluster algorithms. Multi-grid algorithms can lower the critical exponent to $z \approx 0.5-0.7$ [28] for $O(N)$-spin systems. For these systems cluster algorithms are even more efficient ($z \approx 0$).

4.5 The Metropolis algorithm

The Metropolis algorithm is a simple algorithm that can be applied to a wide variety of statistical systems. The transition probability is split into two parts:

$$\begin{aligned} W(S \to S') =& T(S \to S')A(S \to S') \\ &+ \left(1 - \sum_X T(S \to X)A(S \to X)\right)\delta(S, S') \end{aligned} \tag{4.18}$$

Where $T(S \to S')$ is the probability to propose a transition from configuration S to configuration S' and $A(S \to S')$ is the probability to accept this proposal. The second term in (4.18) guarantees compliance with the normalization (4.3). T and A fulfill:

$$\sum_{S'} T(S \to S') = 1 \tag{4.19}$$

$$T(S \to S') = T(S' \to S) \tag{4.20}$$

$$A(S \to S') = \min\left(1, \exp\left[-\frac{1}{k_B T}(H(S') - H(S))\right]\right), \tag{4.21}$$

and hence the algorithm satisfies detailed balance. Whether the algorithm is ergodic or not depends on the form of T. For simulations of the XY model T can be chosen as follows:

$$T(S \to S') = \prod_{m=1}^{V} t_m(\vec{s}_m \to \vec{s}_m{}') \tag{4.22}$$

$$t_m(\vec{s}_m \to \vec{s}_m{}') = \begin{cases} \frac{1}{2\alpha_0} & |\arccos(\vec{s}_m \cdot \vec{s}_m{}')| \leq \alpha_0 \\ 0 & \text{else} \end{cases} \tag{4.23}$$

In such a sweep a proposal is made for every site m. The proposal is to rotate the appropriate spin $\vec{s}_m$ by an angle $\alpha \in (-\alpha_0, \alpha_0)$. The parameter α_0 can be chosen freely but a choice where the acceptance probability lies around 0.5 is favorable.

4.6 Cluster algorithms

Cluster algorithms are related to percolation theory [29]. R.H. Swendsen and J-Sh. Wang [30] were the first to recognize this connection and proposed a cluster algorithm for the Ising model and for q-states models. U. Wolff [31] put forward a cluster algorithm for $O(N)$ spin systems generalizing the spin-flip operation of the Ising model. Unfortunately so far it has been impossible to develop efficient cluster algorithms for spin glasses or gauge theories. A good review on cluster algorithms is given by [32]

4.6.1 Single cluster algorithm

An update in a single cluster algorithm for the XY model in two dimensions (3.5) consists of the following steps:

1. A direction in the $\mathbb{R}^2$ plane is chosen randomly. It is represented by the unit vector $\vec{r}$

2. From the square lattice Λ with $|\Lambda| = L \times K$ sites, one site $x \in \Lambda$ is chosen randomly and added to the cluster $C \subset \Lambda$.

3. All neighbors y of x are added to the cluster C with the probability $p_{\vec{r}}(\vec{s}_x, \vec{s}_y) = 1 - e^{\min[0,\ -2\beta \vec{s}_x \cdot \vec{r}\ \vec{s}_y \cdot r]}$ and x is marked as "already processed".

4. Step three is repeated recursively for all $x \in C$, that are not marked as "already processed".

5. Finally the system is updated. A configuration S is transformed into $S' = R_{\vec{r},C}(S)$, where $R_{\vec{r},C}(S)$ means that for each site belonging to the cluster the associated spin is reflected on the plane perpendicular to $\vec{r}$:

$$\vec{s}_x\,' = \begin{cases} \vec{s}_x - 2(\vec{s}_x \cdot \vec{r})\vec{r} & x \in C \\ \vec{s}_x & x \notin C \end{cases} \tag{4.24}$$

This algorithm is ergodic, because at least one site is updated and this site is selected randomly. A proof of detailed balance can be found in appendix A.2.

4.6.2 Multi cluster algorithm

Instead of creating only one cluster the whole lattice can be subdivided into clusters which then can be updated independently. For the XY model an update would look as follows:

1. A direction in the $\mathbb{R}^2$ plane is chosen randomly. It is represented by the unit vector $\vec{r}$

2. On each link (connection between two neighbors) of the lattice a bond is placed with the probability $p_{\vec{r}}(\vec{s}_x, \vec{s}_y) = 1 - e^{\min[0,\ -2\beta \vec{s}_x \cdot \vec{r}\ \ \vec{s}_y \cdot \vec{r}]}$

3. The resulting bond configuration is decomposed into a set of clusters that are not connected to each other.

4. Each cluster is updated with a probability of 50%. The update procedure is the same as in the single cluster case.

The decomposition into clusters can be performed by applying a Hoshen-Kopelman algorithm [33] or a tree search. Figure 4.1 shows a typical Monte Carlo configuration of the XY model. The biggest cluster is emphasized.

The single cluster algorithm has got the advantage that big clusters are updated more frequently [32], which makes it more efficient than the multi cluster algorithm. Therefore this algorithm was used to obtain all the results in chapter 7.

4.7 Improved estimators

The average of an observable $A(\phi)$

$$\langle A \rangle = \frac{\int D\phi\ \exp[-H(\phi)]A(\phi)}{\int D\phi\ \exp[-H(\phi)]} = \frac{1}{Z}\int D\phi\ \exp[-H(\phi)]A(\phi) \tag{4.25}$$

shall be estimated with a Monte Carlo simulation. When the integral can be split into two parts ($\phi = (\theta, \psi)$), a conditional average, extending over one of these variables can be introduced:

$$\langle A \rangle_{\mathrm{cond}}(\theta) := \frac{1}{Z_{\mathrm{cond}}}\int D\psi\ \exp[-H_{\mathrm{cond}}(\psi)]A(\theta,\psi)\,, \tag{4.26}$$

with $H_{\mathrm{cond}}(\psi) = H(\theta,\psi)|_{\theta=\mathrm{fixed}}$ and $Z_{\mathrm{cond}}(\theta) = \int D\psi\ \exp[-H_{\mathrm{cond}}(\psi)]$. Then averages can be rewritten:

$$\begin{aligned}
\langle A \rangle &= \frac{1}{Z}\int D\theta\, D\psi\ \exp[-H(\theta,\psi)]A(\theta,\psi) \\
&= \frac{1}{Z}\int D\theta\, \frac{\int D\psi\ \exp[-H(\theta,\psi)]A(\theta,\psi)}{\int D\psi'\ \exp[-H(\theta,\psi')]}\int D\psi'\ \exp[-H(\theta,\psi')] \\
&= \frac{1}{Z}\int D\theta\, \frac{1}{Z_{\mathrm{cond}}}\int D\psi\ \exp[-H_{\mathrm{cond}}(\psi)]A(\theta,\psi)\int D\psi'\ \exp[-H(\theta,\psi')] \\
&= \frac{1}{Z}\int D\theta\, D\psi'\ \exp[-H(\theta,\psi')]\langle A \rangle_{\mathrm{cond}} \\
&= \langle A_{\mathrm{imp}} \rangle
\end{aligned} \tag{4.27}$$

In the last step the improved estimator A_{imp} was introduced as the conditional average of A that depends only on θ. It has the same expectation value as A.

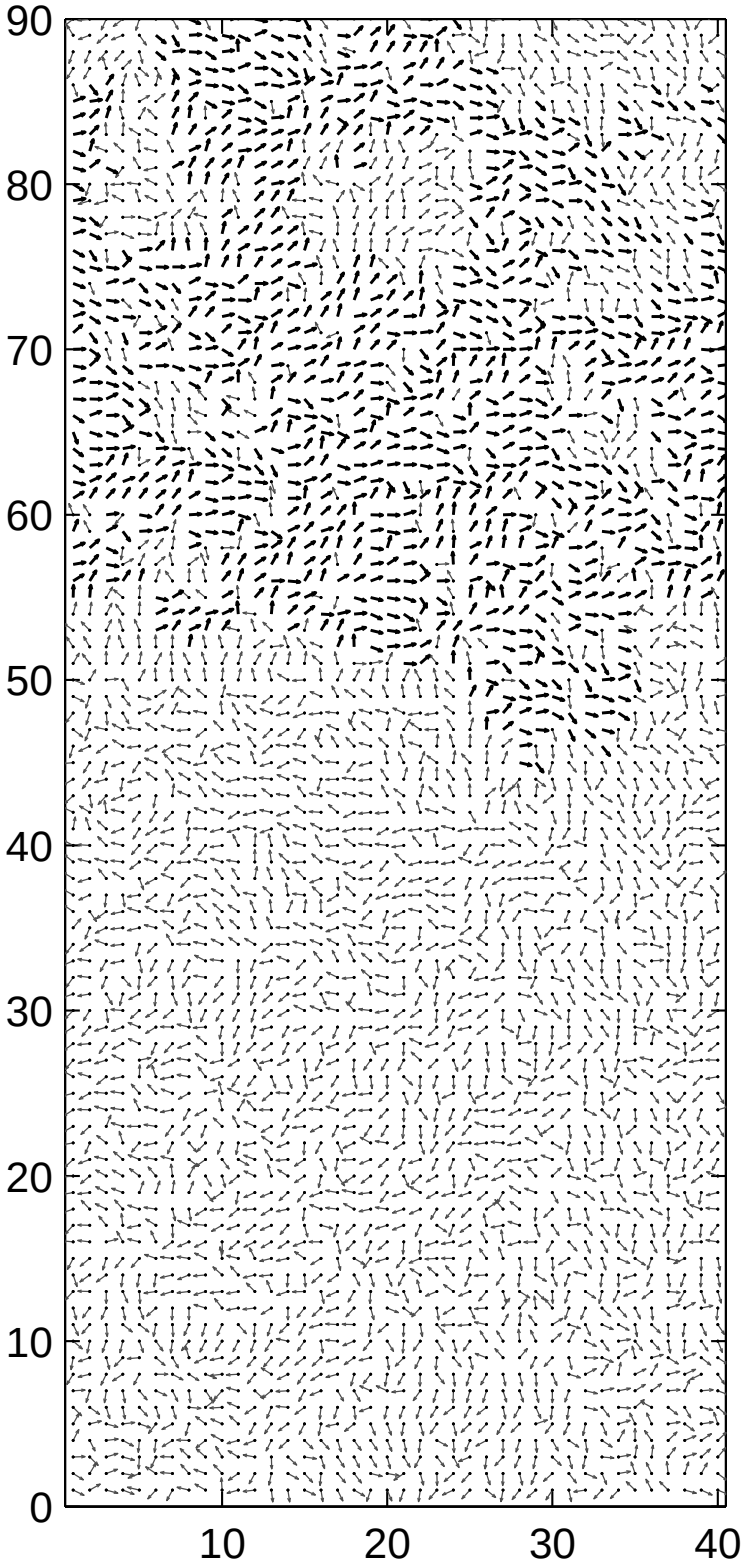

Figure 4.1: A typical configuration at $\beta = 1.0$. The biggest cluster is emphasized

If the ψ-integrals were performed exactly a lot would be gained because the variance of the improved estimator is smaller than the variance of the original observable (for a proof see A.3):

$$\langle A^2\rangle - \langle A\rangle^2 \geq \langle A_{\text{imp}}^2\rangle - \langle A_{\text{imp}}\rangle^2 \tag{4.28}$$

4.7.1 Hasenbusch improved estimator

In the XY-model with standard action (lattice units)

$$H = -\beta \sum_{x,t} (\vec{s}(x,t)\cdot\vec{s}(x+1,t) + \vec{s}(x,t)\cdot\vec{s}(x,t+1)) \tag{4.29}$$

on a lattice of size $L \times K$ with periodic boundary conditions in the space direction and free boundary conditions in the time direction, the Hasenbusch improved estimator [19] can be applied to measure the *time slice correlation function*

$$G(\tau) = \vec{S}(t)\cdot\vec{S}(t+\tau)\,, \tag{4.30}$$

$$\vec{S}(t) = \frac{1}{L}\sum_x \vec{s}(x,t) \tag{4.31}$$

From this function the finite volume massgap (2.24) of the theory and consequently the LWW-coupling (2.31) can be obtained.

The idea is to perform the same $O(2)$ transformation on all spins of a given time slice: $\forall x : \vec{s}(x,t) \to \mathbf{R}(t)\vec{s}(x,t)$. The integral over all $O(2)$-matrices $\mathbf{R}(t)$ can be performed analytically which yields the improved estimator.

The conditional action, which depends on $\mathbf{R}(t)$ is

$$H_{\text{cond}} = -\beta \sum_{x,t} (\mathbf{R}(t)\vec{s}(x,t))\cdot(\mathbf{R}(t+1)\vec{s}(x,t+1)) \tag{4.32}$$

Contributions from within a time slice were dropped because they do not depend on $\mathbf{R}$ and result only in a constant factor that does not influence any average.

The action can be expressed in terms of relative rotations:

$$\mathbf{X}(t,t+1) = \mathbf{R}^{-1}(t)\mathbf{R}(t+1) \tag{4.33}$$

To achieve this, $\mathbf{R}^{-1}(t)$ is applied from the left on both vectors (This oper-

ation does not change the dot products):

$$\begin{aligned} H_{\rm cond} &= -\beta \sum_{x,t} \left(\mathbf{R}^{-1}(t)\mathbf{R}(t)\vec{s}(x,t)\right) \cdot \left(\mathbf{R}^{-1}(t)\mathbf{R}(t+1)\vec{s}(x,t+1)\right) \\ &= -\beta \sum_{x,t} \vec{s}(x,t) \cdot (\mathbf{X}(t,t+1)\vec{s}(x,t+1)) \\ &= -\beta \sum_{x,t} \sum_{\alpha,\gamma=1}^{2} X_{\alpha\gamma}(t,t+1) s_\alpha(x,t) s_\gamma(x,t+1) \\ &= -\beta \sum_{t} \sum_{\alpha,\gamma} X_{\alpha\gamma}(t,t+1) Q_{\alpha\gamma}(t,t+1) \end{aligned} \tag{4.34}$$

In the last step

$$Q_{\alpha\gamma}(t,t+1) = \sum_x s_\alpha(x,t) s_\gamma(x,t+1) \tag{4.35}$$

was introduced. The partition function factorizes into:

$$Z_{\rm cond} = \prod_t z(t,t+1) \tag{4.36}$$

with the time-slice partition functions

$$z(t,t+1) = \int dX \, \exp\left[-\beta \sum_{\alpha\gamma} X_{\alpha\gamma}(t,t+1) Q_{\alpha\gamma}(t,t+1)\right] \tag{4.37}$$

The integration extends over all $X(t,t+1) \in O(2)$ (Haar-measure). The improved estimator for $G(\tau)$ is given by:

$$\begin{aligned} G_{\rm imp}(\tau) &= \langle G(\tau) \rangle_{\rm cond} \\ &= \frac{\int \left(\prod_t dR(t)\right) \, e^{-H_{\rm cond}} \mathbf{R}(t)\vec{S}(t) \cdot \mathbf{R}(t+\tau)\vec{S}(t+\tau)}{Z_{\rm cond}} \end{aligned} \tag{4.38}$$

Expressing all $\mathbf{R}$ by relative rotations yields:

$$\begin{aligned} G_{\rm imp}(\tau) &= \left\langle \vec{S}(t) \cdot \mathbf{X}(t,t+\tau)\vec{S}(t+\tau) \right\rangle_{\rm cond} \\ &= \sum_{\alpha,\gamma} S_\alpha(t) \left\langle X_{\alpha\gamma}(t,t+\tau) \right\rangle_{\rm cond} S_\gamma(t+\tau) \end{aligned} \tag{4.39}$$

The expectation value can be written as a matrix product:

$$\langle \mathbf{X}(t',t'+\tau) \rangle_{\rm cond} = \prod_{t' \le t < t'+\tau} \tilde{\mathbf{X}}(t,t+1) \tag{4.40}$$

with the time slice averages:

$$\tilde{\mathbf{X}}(t,t+1) = \frac{\int dX \, \exp\left(\sum_{\alpha,\gamma} X_{\alpha\gamma}(t,t+1) Q_{\alpha\gamma}(t,t+1)\right) \mathbf{X}(t,t+1)}{z(t,t+1)} \tag{4.41}$$

Performing the integration exactly (Appendix A.4) finally gives:

$$\tilde{X}_{11}(t,t+1) = \tilde{X}_{22}(t,t+1) = \frac{Q_{11}+Q_{22}}{\kappa}\frac{I_1(\kappa)}{I_0(\kappa)} \tag{4.42}$$

$$\tilde{X}_{21}(t,t+1) = -\tilde{X}_{12}(t,t+1) = \frac{Q_{21}-Q_{12}}{\kappa}\frac{I_1(\kappa)}{I_0(\kappa)} \tag{4.43}$$

where I_0 and I_1 are modified Bessel functions and

$$\kappa = \sqrt{(Q_{11}+Q_{22})^2 + (Q_{21}-Q_{12})^2}. \tag{4.44}$$

This estimator has been shown to greatly lower the variance, especially near the KT-phase transition [19].

4.8 Tests

To make sure that the algorithms were implemented correctly several tests were carried out.

4.8.1 Equilibration

It is important to make sure that runs from different starting configurations lead to compatible results. In addition some information about the equilibration time can be obtained from these runs. The following two starting configurations were employed to test the algorithms:

1. All spins point to the left (cold start).
2. The directions of the spins are distributed randomly (hot start).

An example is given in figure 4.2. Equilibrium is reached faster from the cold start, because at low temperatures neighboring spins tend to line up and the energy is an $O(n)$ invariant observable.

Thorough studies have shown that all used algorithms pass this test.

4.8.2 Comparison with a known observable

Sometimes the value of a non trivial observable is known exactly. To check whether the algorithms reproduce this value within the statistical errors is a very good test.

For the Metropolis algorithm it is known that (a proof can be found in A.5):

$$\left\langle e^{-\beta\Delta H} \right\rangle = 1\,, \tag{4.45}$$

where $\Delta H = H(S') - H(S)$ is the energy difference between the proposed and the current configuration. Table 4.1 shows that the implemented Metropolis algorithm passes this test.

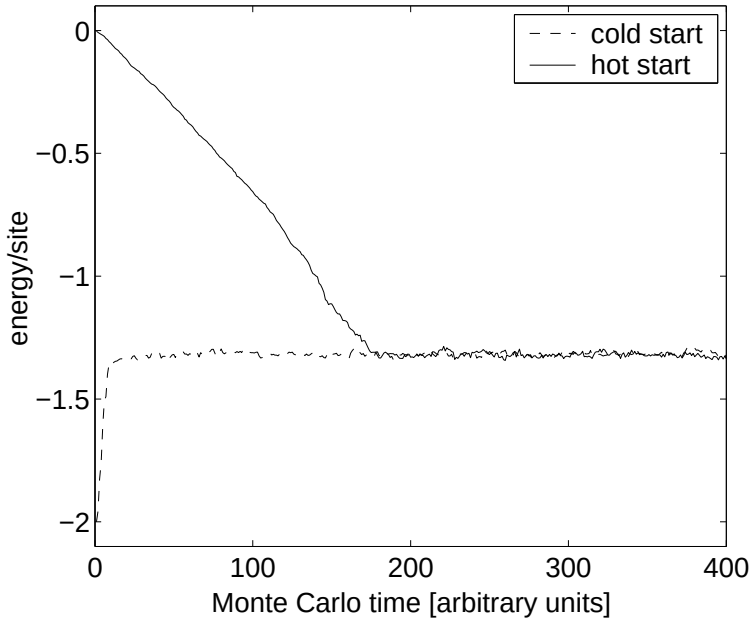

Figure 4.2: Energy/site is plotted against the Monte Carlo time. The plotted simulations were done on a 128×128 lattice at $\beta = 1.0$ with the single cluster algorithm.

β	$L \times K$	$< e^{-\beta \Delta H} >$
0.82	56×56	1.00025 ± 0.00015
0.86	128×128	0.99991 ± 0.00008
0.88	128×128	1.00004 ± 0.00008
0.90	128×128	0.99996 ± 0.00009
1.50	32×32	1.0001 ± 0.0002
1.50	64×64	0.9995 ± 0.0010

Table 4.1: Measurements of $< e^{-\beta \Delta H} >$ on a lattice of size $L \times K$.

4.8.3 Comparison with former results

A lot of results were obtained for the XY model in the past. In a final test some of the available data [34] was reproduced with my version of the cluster algorithm. The results are summarized in table 4.2.

β	$L \times K$	χ	χ_{ref}	ξ	ξ_{ref}
0.82	56×56	36.4(3)	36.33(14)	4.39(6)	4.315(27)
0.86	128×128	60.9(5)	59.85(26)	5.83(4)	5.843(38)
0.88	128×128	80.1(6)	80.58(31)	6.96(4)	7.011(40)
0.90	128×128	111(1)	111.43(44)	8.4(1)	8.476(66)
0.92	128×128	164(2)	162.68(61)	10.65(6)	10.69(8)
0.96	128×128	421(5)	414.1(1.7)	18.4(2)	18.08(13)

Table 4.2: Comparison of the susceptibility χ and the correlation length ξ with Wolff's results χ_{ref} and ξ_{ref} in the vortex phase

At the critical coupling $\beta_c \approx 1.1197(5)$ [19] Kosterlitz Thouless theory predicts how the continuum value of the LWW-coupling is reached [35]:

$$2M(L)L|_{\beta_c} = \frac{\pi}{2} - \frac{\pi}{4}\frac{c}{1 - c\,\ln\left(\frac{a}{L}\right)} \tag{4.46}$$

L is the volume of the system, $M(L)$ is the finite volume massgap, a is the lattice constant and c is a non universal constant to be found. In Figure 4.3 results obtained with the single cluster algorithm are plotted (the data can be obtained from appendix B.3).

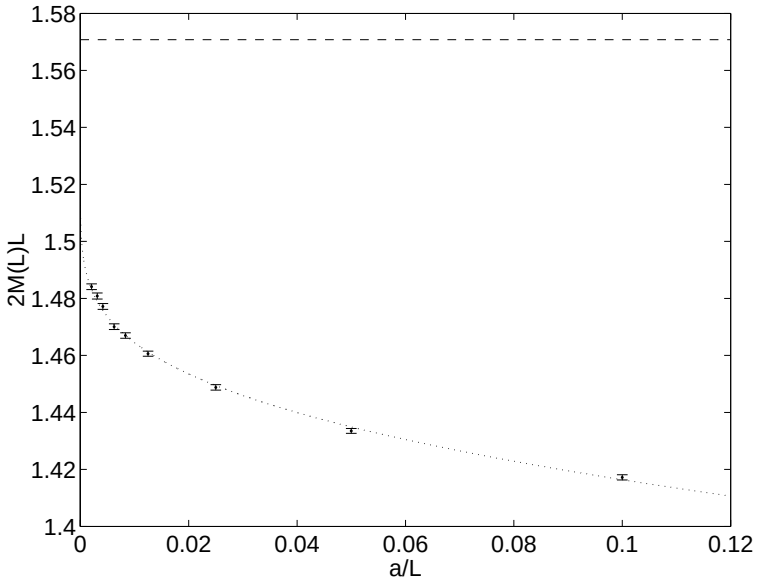

Figure 4.3: Approach of $\bar{g}^2(L) = 2M(L)L$ to the continuum at β_c

A least square fit of the data yields:

$$c = 0.3592 \pm 0.0023 \tag{4.47}$$

which agrees with the result obtained in [35].

Chapter 5

The DdV equation

5.1 Theory

In this section a 6-vertex model is introduced, which describes the scattering of massless chiral fermions. When the thermodynamic limit is taken, the equations of motion are those of the massive Thirring model, which (under certain assumptions) is equivalent to the sine Gordon model [24]. A mapping between vertex models and spin chains is known [36]. The S-matrix of the 6-vertex model is deeply related with the transfer matrix of the XXZ(1/2) chain which can be diagonalized with Bethe ansatz method. To find the Bethe roots a nonlinear integral equation must be solved. As the sine Gordon model is believed to be suitable to describe the critical properties of the XY model, this result can be used to calculate the finite volume massgap and thus the LWW coupling of the nonlinear $O(2)$ $\sigma-$model.

5.1.1 QFT on a light cone lattice

Usually when space time is discretized either a Hamiltonian lattice is introduced where space is discrete and time is continuous, or an Euclidean lattice where both space and time are discrete. In the latter sites are connected along the coordinate axes. Another possibility is a light cone lattice where links between two sites (events) are placed along the light cone directions (fig. 5.1).

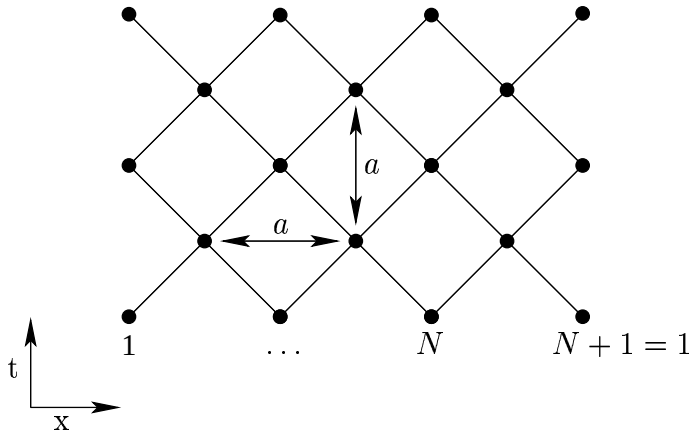

Figure 5.1: A light cone lattice in two dimensions

Let the lattice have N sites and periodic boundary conditions in the space direction and be of infinite extent in the time direction. Massless, free particles can be associated with each site i which are called left movers (L) and right movers (R). They are represented by asymptotic states $|\alpha_{Li}, \alpha_{Ri}\rangle = |\alpha_{2i-1}, \alpha_{2i}\rangle$ (fig. 5.2) that live on the links. This states are vectors in a Hilbert space which factorizes into:

$$\mathcal{H}_i = \mathcal{H}_{Li} \otimes \mathcal{H}_{Ri} \tag{5.1}$$

The total Hilbert space is:

$$\mathcal{H}_N = \bigotimes_{i=1}^{N} \mathcal{H}_i \tag{5.2}$$

with states:

$$|\alpha\rangle = |\alpha_1, \alpha_2\rangle \otimes \cdots \otimes |\alpha_{2N-1}, \alpha_{2N}\rangle \in \mathcal{H}_N \tag{5.3}$$

At every site a whole process can happen which is described by the transition amplitude (S-matrix element):

$${}_{\text{out}}\langle \beta_L, \beta_R | \alpha_R, \alpha_L \rangle_{\text{in}} = S^{\beta_R, \beta_L}_{\alpha_R, \alpha_L} \tag{5.4}$$

This matrix describes $2 \to 2$ particles scattering. It is assumed that a general $m \to n$ particles scattering can be factorized into $2 \to 2$ particles scatterings.

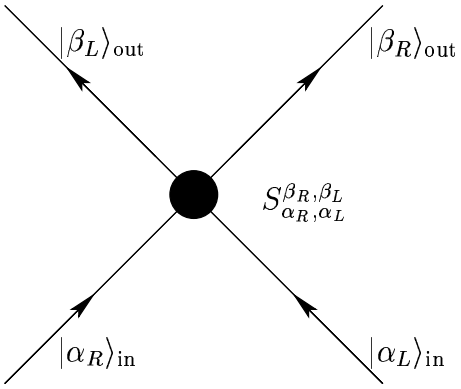

Figure 5.2: The S matrix

A connection with thermodynamics occurs, when the extension in the time direction is also chosen to be finite. Then there exist initial and final states $|\alpha\rangle_{\text{in}}$ and $|\beta\rangle_{\text{out}}$. The total transition amplitude is given by:

$$Z := {}_{\text{out}}\langle\beta|\alpha\rangle_{\text{in}} = \sum_{\text{int.states}} \prod_{\text{sites}} S_{\gamma',\gamma''}\,, \tag{5.5}$$

where γ' and γ'' are internal states. $S_{\gamma',\gamma''}$ is real and positive and plays the role of a Boltzmann weight in a statistical system with its partition function given by (5.5). This correspondence was first recognized by A.B. Zamolodchikov in [37]. Boltzmann weights are usually written down in a slightly different notation:

$$R^{\beta_R,\beta_L}_{\alpha_L,\alpha_R} = S^{\beta_R,\beta_L}_{\alpha_R,\alpha_L}. \tag{5.6}$$

When the particles are assumed to be fermions without internal degrees of freedom (color), then due to Pauli's exclusion principle only one particle of type R and one of type L can can exist on the same site. When the number of the particles is to be conserved, the 6-vertex model is obtained. The only possible amplitudes are:

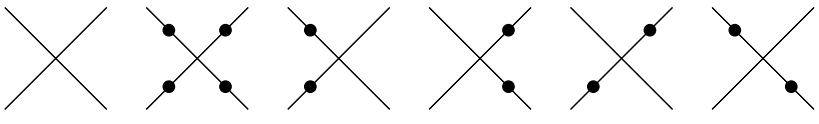

Figure 5.3: Non vanishing S matrix elements

The R matrix has only 6 non vanishing entries:

$$R(\theta,\gamma) = \begin{pmatrix} a & & & \\ & c & b & \\ & b & c & \\ & & & a \end{pmatrix} \tag{5.7}$$

A row-to-row transfer matrix t can be defined. It is the product of concatenated $R-$ matrices along a whole horizontal line of the lattice. The XXZ(1/2) chain is defined by the Hamiltonian

$$H = \sum_{i=1}^{N} [\sigma_x^i \sigma_x^{i+1} + \sigma_y^i \sigma_y^{i+1} + (1-\cos\gamma)\sigma_z^i \sigma_z^{i+1}] \tag{5.8}$$

The σ are Pauli matrices and γ is the anisotropy. The transfer matrix of the vertex model is given by an exponential of the XXZ(1/2) Hamiltonian

$$t^{(N)} = e^{-H} \tag{5.9}$$

5.1.2 Bethe Ansatz and DdV equations

The Bethe ansatz [38] is a method to diagonalize the transfer matrix. It is stated, that there exists a reference state $|\Omega\rangle$ and operators $B(\theta)$ and $C(\theta)$ are introduced such that

$$B(\theta_1)\cdots B(\theta_M)|\Omega\rangle \tag{5.10}$$

is an eigenstate of the transfer matrix for an appropriate choice of θ_j and

$$C(\theta)|\Omega\rangle = 0 \tag{5.11}$$

When the θ_j can be found the transfer matrix is diagonalized. They can be obtained from a set of M coupled nonlinear equations - the Bethe Ansatz equations. The Bethe Ansatz equations can be rewritten in terms of a counting function which contains the information about the Bethe roots θ_j:

$$Z_N(\theta_j) = 2\pi I_j\,, \tag{5.12}$$

where the I_j plays the role of a quantum number:

$$I_j = \mathbb{Z} + \frac{1+\delta}{2}\,, \tag{5.13}$$

and $\delta \in 0,1$ is zero when $N-S$ is even and one else. S is the third component of the spin of the chain in the given state. Instead of solving the Bethe Ansatz equations, equivalent nonlinear integral equations for the counting function can be solved. These equations were derived for the ground state of the sine Gordon theory by C. Destri and de H.J. Vega (DdV-equations) [39]. The equations for excited states were found in [40] [41] [42].

For the lowest two states the continuum versions of the DdV equations are given in the next section and solved numerically in section 5.2.

5.1.3 The massgap in the XY model

The finite volume massgap $M(L) = E_1(L) - E_0(L)$ in the sine Gordon theory can be calculated [4] by solving the DdV equations. The ground state energy in finite volume is:

$$E_0(L) = -\frac{M}{\pi} \operatorname{Im} \int_{-\infty}^{+\infty} dx \ \sinh(x + i\eta) \ \ln\left[1 + e^{iZ_0(x+i\eta)}\right] \tag{5.14}$$

where M is the infinite volume massgap and L is the extension of the system. The counting function $Z_0(\theta)$ is a solution of the nonlinear integral equation:

$$\begin{aligned} Z_0(\theta) = {} & ML \sinh\theta \\ & + i \int_{-\infty}^{+\infty} dx \ [G(\theta - x - i\eta) - G(\theta + x + i\eta)] \ln\left[1 + e^{iZ_0(x+i\eta)}\right] \end{aligned} \tag{5.15}$$

The energy of the first excited state is given by:

$$E_1(L) = M - \frac{M}{\pi} \operatorname{Im} \int_{-\infty}^{+\infty} dx \ \sinh(x + i\eta) \ \ln\left[1 - e^{iZ_1(x+i\eta)}\right] , \tag{5.16}$$

with $Z_1(\theta)$ being a solution of:

$$\begin{aligned} Z_1(\theta) = {} & ML \sinh\theta + \chi(\theta) \\ & + i \int_{-\infty}^{+\infty} dx \ [G(\theta - x - i\eta) - G(\theta + x + i\eta)] \ln\left[1 - e^{iZ_1(x+i\eta)}\right] \end{aligned} \tag{5.17}$$

The source term $\chi(\theta)$ is of the form:

$$\chi(\theta) = 2\pi \int_0^{\theta} dz \, G(z). \tag{5.18}$$

The integrals are independent of η as long as $0 < \eta < \pi$ (This is shown in appendix A.6). The kernel is given by:

$$G(\theta) = \frac{1}{2\pi} \int_{-\infty}^{+\infty} dk \ e^{ik\theta} \ \frac{\sinh\frac{\pi k(p-1)}{2}}{2\cosh\frac{\pi k}{2}\sinh\frac{\pi kp}{2}}. \tag{5.19}$$

The XY model is believed to lie in the same universality class as the sine Gordon model with the sG coupling $\beta_{\rm SG} = \sqrt{8\pi}$, or $p \to \infty$ [22]. In this case the kernel simplifies:

$$\begin{aligned} G(\theta) &= \frac{1}{2\pi}\int_{-\infty}^{+\infty} dk\; e^{ik\theta}\;\left(\frac{1}{2} - \frac{1}{2}\,\mathrm{sign}\,k\,\tanh\frac{\pi k}{2}\right) \\ &= \frac{1}{2\pi}\int_{-\infty}^{+\infty} dk\,\frac{e^{ik\theta}}{e^{\pi|k|}+1} \end{aligned} \tag{5.20}$$

The Fourier transformation can be carried out:

$$G(\theta) = \frac{1}{4\pi^2}\left(-\Psi(\frac{\pi - i\theta}{2\pi}) - \Psi(\frac{\pi + i\theta}{2\pi}) + \Psi(1 - \frac{i\theta}{2\pi}) + \Psi(1 + \frac{i\theta}{2\pi})\right) \tag{5.21}$$

$\Psi(z)$ is the digamma function[1]. The kernel is plotted in fig. 5.4

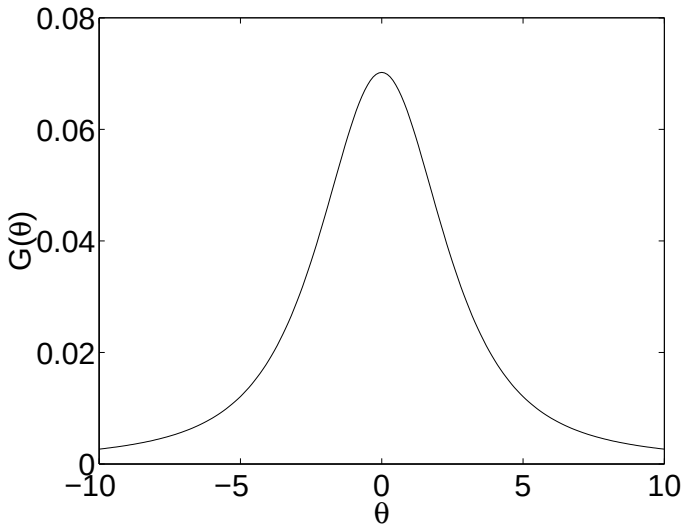

Figure 5.4: The kernel $G(\theta)$ for $\theta \in \mathbb{R}$.

Also the source term can be calculated exactly in the limit $p \to \infty$. It can be written as a sum of gamma functions:

$$\begin{aligned} \chi(x + i\eta) = &- i\,\ln\left[\Gamma\left(0.5 - \frac{ix-\eta}{2\pi}\right)\right] + i\,\ln\left[\Gamma\left(0.5 + \frac{ix-\eta}{2\pi}\right)\right] \\ &+ i\,\ln\left[\Gamma\left(1 - \frac{ix-\eta}{2\pi}\right)\right] - i\,\ln\left[\Gamma\left(1 - \frac{ix-\eta}{2\pi}\right)\right] \end{aligned} \tag{5.22}$$

[1]The digamma function $\Psi(z)$ is the logarithmic derivative of the gamma function, given by $\Psi(z) = \Gamma'(z)/\Gamma(z)$.

5.2 Numerical solution of the DdV equation

To calculate the massgap $m(L)$ it is necessary to solve the DdV equation for $Z_0(\theta)$ and for $Z_1(\theta)$. The integrands are nearly zero for large arguments so the integration can be restricted to an interval $[-cut, cut]$. How big this interval has to be depends on the chosen volume L and must be explored carefully. This interval is covered by a finite number of sampling points and standard numerical integration methods (e.g. Simpson's rule) are applied to evaluate the integrals.

The following iteration procedure can be applied to solve the integral equation numerically [43] (the procedure is presented for the Z_1 case, and can be carried out analogly for Z_0):

- In a first approximation the integral is ignored.

$$Z_1^{(0)}(x+i\eta) = ML\,\sinh(x+i\eta) + \chi(x+i\eta)$$

- To obtain further approximations, the last one is inserted into the integral:

$$\begin{aligned} Z_1^{(1)}(x+i\eta) &= ML\,\sinh(x+i\eta) + \chi(x+i\eta) \\ &\quad + i\int_{-cut}^{+cut} d\xi\ \left[G(x-\xi) - G(x+\xi+2i\eta)\right] \ln\left[1 - e^{iZ_1^{(0)}(\xi+i\eta)}\right] \end{aligned}$$

$$\vdots$$

$$\begin{aligned} Z_1^{(n)}(x+i\eta) &= ML\,\sinh(x+i\eta) + \chi(x+i\eta) \\ &\quad + i\int_{-cut}^{+cut} d\xi\ \left[G(x-\xi) - G(x+\xi+2i\eta)\right] \ln\left[1 - e^{iZ_1^{(n-1)}(\xi+i\eta)}\right] \end{aligned}$$

The iteration stops when the desired accuracy is reached. At small ML the iteration converges slower than at large ones. Results for the massgap had been obtained without any problems in the range $10^{-12} < ML < 10$. Before the solutions can be trusted it is necessary to check whether they are sufficiently independent of the choice of η, cut and the number of sampling points.

5.3 Tests

It was found out that a choice of $cut \approx 10$ is sufficient for $ML \approx 1$ and must be increased for smaller ML (up to $cut \approx 70$ for $ML \approx 10^{-12}$). The solution is almost independent of η, in most calculations a value of $\eta \approx 0.25\ \pi$ was chosen. Simpson's rule was used to perform the integrals. The integrands are smooth enough, so that the solution gets better when the number of sampling points n is increased (error $\propto \left(\frac{1}{n}\right)^4$ with Simpson) until truncation errors become significant. In Figures 5.5 - 5.7 the LWW coupling obtained from the solution of the DdV equation is compared with Lüscher's formula [44]

$$\begin{aligned} 2M(L)L =& 2ML + \frac{2ML}{\pi} \int_{-\infty}^{+\infty} d\theta\ \cosh\theta e^{-ML\cosh\theta} \left[1 + e^{i\chi(\theta+\frac{i\pi}{2})}\right] \\ &+ \mathcal{O}(e^{-2ML}) \end{aligned} \tag{5.23}$$

at large ML and with a short distance expansion [21] [4] at small ML:

$$2M(L)L = \frac{\pi}{2} - \frac{\pi}{4\ln(ML)} + \ldots \tag{5.24}$$

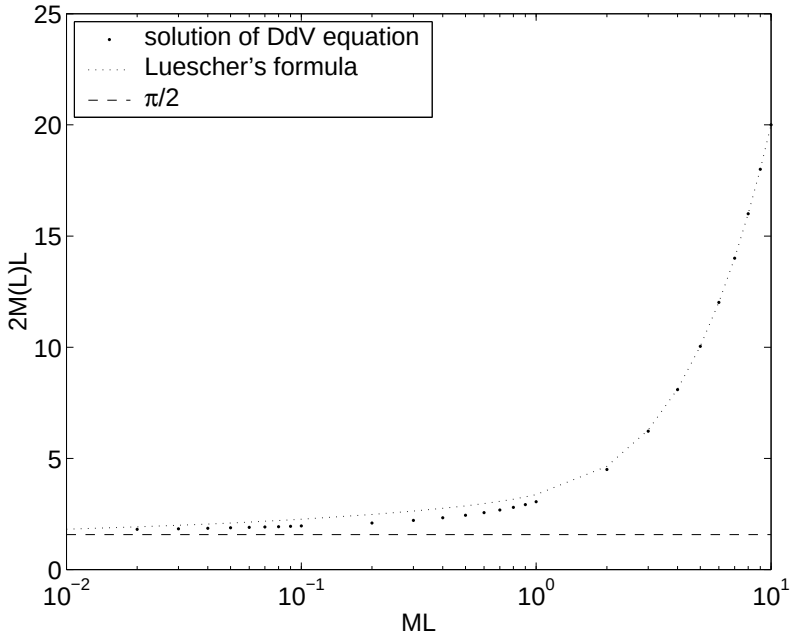

Figure 5.5: LWW coupling obtained from solutions of the DdV equation at large ML

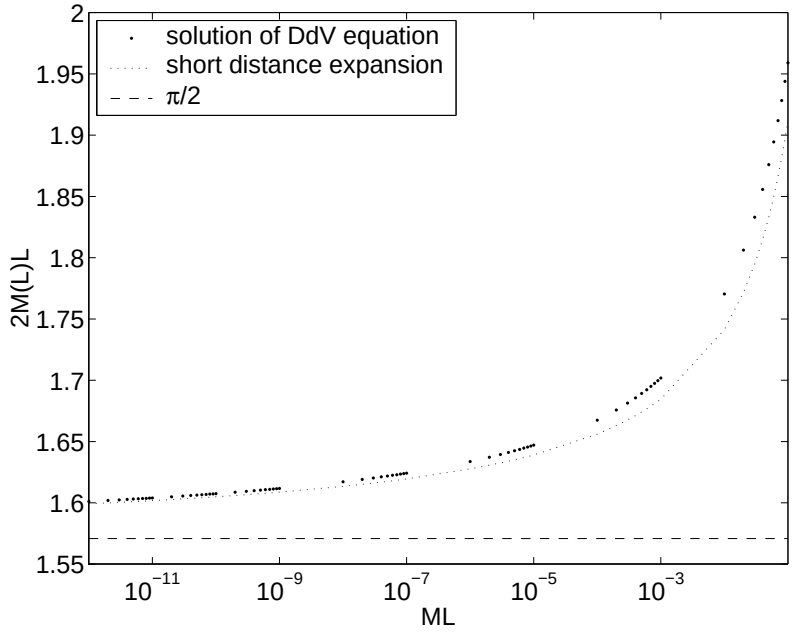

Figure 5.6: LWW coupling obtained from solutions of the DdV equation at small ML

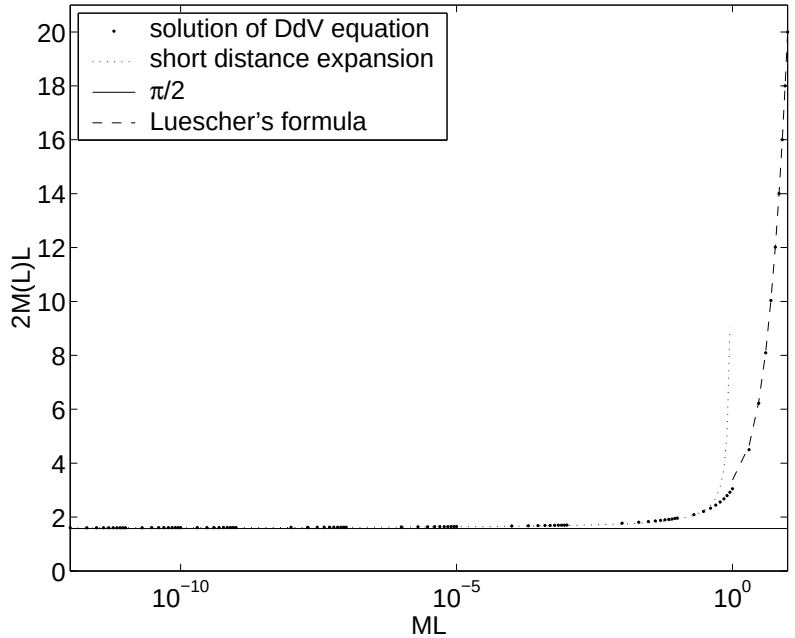

Figure 5.7: LWW coupling obtained from solutions of the DdV equation. Both regions of ML are plotted

Chapter 6

The LWW-coupling

6.1 Measuring the LWW coupling

To calculate the LWW coupling $\bar{g}^2(L) = 2M(L)L$ the massgap $M(L)$ must be measured. This can be obtained from the zero momentum correlation function (4.30). Contributions from higher energy states are suppressed exponentially, which is even enhanced by the application of free boundary conditions (see section 6.1.1). For large time separations the influence of these states is negligible and the correlation function is (all quantities are expressed in lattice units):

$$G(\tau) \approx \exp\left[-\tau(E_1 - E_0)\right] \tag{6.1}$$

The massgap is hence given by the inverse of the correlation length

$$M(L) = E_1 - E_0 = \frac{1}{\xi} = \ln \frac{G(\tau)}{G(\tau+1)} \tag{6.2}$$

Let the lattice have a spatial extent L and a temporal extent $K = 5L$. Periodic boundary conditions are used in the spatial direction and free boundary conditions in the temporal direction. When in a strip of length $3L$ in the middle of the lattice translational invariance is assumed[1], then the correlation function can be estimated as follows:

$$G(\tau) = \left\langle \frac{1}{K - 2L - \tau} \sum_{t=L+1}^{K-L-\tau} \sum_{x,y} \vec{s}(x,t) \cdot \vec{s}(y, t+\tau) \right\rangle_{\text{MC}} \tag{6.3}$$

An estimate for the massgap is given by (6.2) which is a nonlinear function. Hence to estimate the errors jackknife binning is used. When τ is increased $\ln \frac{G(\tau)}{G(\tau+1)}$ reaches a plateau (fig. 6.1), there the contributions from higher energy states are abated and we make contact with the massgap.

[1] Whether this assumption is justified must be carefully checked.

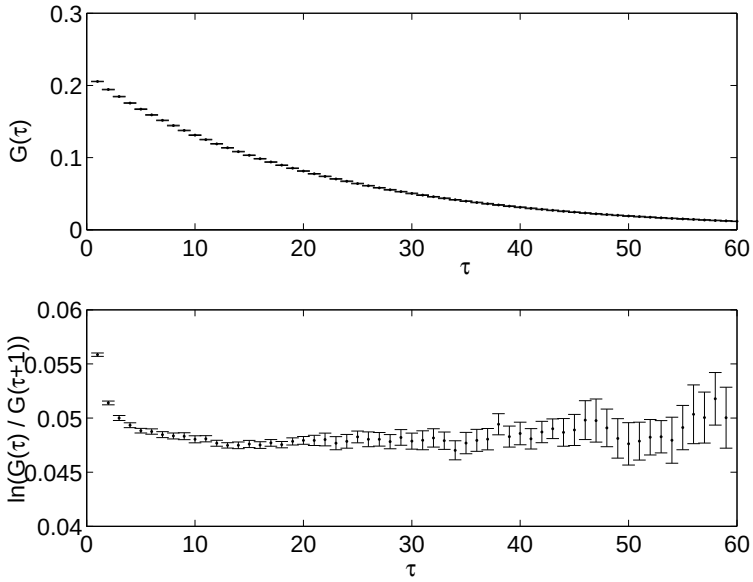

Figure 6.1: The time slice correlation function $G(\tau)$ and the massgap measured at $\beta = 0.97$ on a 60×60 lattice

6.1.1 Free boundary conditions

In section (2.3.1) it was shown that with periodic boundary conditions the partition function of the XY model can be written as:

$$Z = \mathrm{Tr}\ \hat{T}^K\,, \tag{6.4}$$

where $\hat{T}$ is the transfer matrix operator. To calculate the massgap from the time slice correlation function $G(\tau)$ (according to eq. (2.30)) both τ and K have to be large. Only then the influence of higher Energy states may be neglected.

Dirichlet boundary conditions could be chosen as well:

$$\vec{s}(x,1) = \vec{s}_1(x) \tag{6.5}$$
$$\vec{s}(x,T) = \vec{s}_2(x) \tag{6.6}$$

The partition function with Dirichlet boundary conditions is:

$$Z = \int \left(\prod_{t=2}^{K-1} Ds(t)\ T(t+1,t) \right) T(2,1) = \langle s_2 | \hat{T}^{K-2} | s_1 \rangle \tag{6.7}$$

Yet another possibility is to define wave functionals:

$$\phi[\vec{s}(x)] = \langle s|\phi\rangle \tag{6.8}$$
$$\psi[\vec{s}(x)] = \langle s|\psi\rangle \tag{6.9}$$

and define the partition function by:

$$\begin{aligned} Z &= \langle\psi|\hat{T}^{K-2}|\phi\rangle \qquad (6.10)\\ &= \int Ds(1)Ds(T)\ \psi^*[\vec{s}(x,T)]\phi[\vec{s}(x,1)] \\ &\qquad \int \left(\prod_{t=2}^{K-1} Ds(t)\ T(t+1,t)\right) T(2,1) \qquad (6.11) \end{aligned}$$

Free boundary conditions correspond to a choice of $\psi = \phi = \text{const}$. In [2] it was argued that since $|\psi\rangle$ and $|\phi\rangle$ are $O(2)$ invariant, the intermediate states also have to be $O(2)$ invariant. The energies of these states differ by at least $4\pi/L$. Both the ground state and the first excited state are $O(2)$ invariant.

If there was a state with an energy only slightly higher than E_1, the plateau where $\ln[G(\tau)/g(\tau+1)]$ corresponds to the massgap would be reached at a very large τ, where statistical errors are big. Applying free boundary conditions ensures that the difference between E_1 and the next occurring state is large enough.

Implementing free boundary conditions in a Monte Carlo algorithm is quite straight forward. The spins in the first (last) time slice do not have neighbors in the negative (positive) time direction.

6.2 Measuring the step scaling function

The step scaling function $\sigma(2, \bar{g}^2(L)) = \bar{g}^2(2L)$ is to be measured at a certain point of the LWW coupling $\bar{g}^2(L) = u$. Only finite lattices with the lattice spacing a are accessible to numerical simulations, consequently only the lattice version of the step scaling function $\Sigma(2, u, a/L)$ can be measured. Results from different lattices have to be extrapolated to the continuum where:

$$\lim_{a/L\to 0} \Sigma(2, u, a/L) = \sigma(2, u) \qquad (6.12)$$

At each lattice of size L/a the bare coupling β has to be tuned in such a way that the desired value u of the LWW coupling is obtained. Then at the same bare coupling the LWW coupling is measured on a lattice of size $2L/a$ which gives a point of $\Sigma(2, u, a/L)$.

The tuning requires a lot of measurements (and time). In principle the zero of the function $\bar{g}^2(\beta) - u$ is searched, which can be obtained by carrying out the bisection procedure manually.

A systematic error occurs, because the desired value of u can only be achieved with finite accuracy. Let Δu denote the deviation of the Monte Carlo average $\bar{g}^2(L)$ from u:

$$\bar{g}^2(L) = u + \Delta u \qquad (6.13)$$

then for small Δu error propagation yields:

$$\Delta\Sigma_{\text{sys}} \approx \left.\frac{\partial\Sigma}{\partial\bar{g}^2}\right|_u \Delta u. \tag{6.14}$$

The required derivative of Σ can be approximated numerically.

In a similar way the statistical error of $\bar{g}^2(L)$ is taken into account:

$$\Delta\Sigma_{\text{MC1}} \approx \left.\frac{\partial\Sigma}{\partial\bar{g}^2}\right|_u \Delta\bar{g}^2_{\text{MC}}. \tag{6.15}$$

These errors have to be combined with the own statistical error$\Delta\Sigma_{\text{MC2}}$. The final result is:

$$\Sigma(2,u,a/L) = \Sigma(2,u+\Delta u,a/L) + \Delta\Sigma_{\text{sys}} \pm \sqrt{\Delta\Sigma^2_{\text{MC1}} + \Delta\Sigma^2_{\text{MC2}}} \tag{6.16}$$

6.3 Continuum values of the step scaling function

The DdV equations predict the finite volume energy levels of the XY model, thus it is possible to calculate the LWW-coupling in continuum at a given ML (where M is the infinite volume massgap and L the spatial extension):

$$\bar{g}^2(ML) = 2(E_1(ML) - E_0(ML))L \tag{6.17}$$

The continuum value of the step scaling function is given by:

$$\sigma(2,\bar{g}^2(ML)) = 2(E_1(2ML) - E_0(2ML))2L \tag{6.18}$$

This theoretical prediction can be compared with a continuum extrapolation of Monte Carlo estimates for the lattice step scaling function

$$\Sigma(2,u,\frac{a}{L}) \qquad \text{at} \qquad u = \bar{g}^2(ML). \tag{6.19}$$

6.4 Lattice artifacts of the step scaling function

The LWW-coupling $\bar{g}^2 = 2M(L)L$ on a lattice is affected by lattice artifacts. The predicted approach to the continuum is [45]:

$$\bar{g}^2(ML,\xi) = \bar{g}^2(ML,\infty) - \frac{f_1(ML)\pi^2}{2(\ln\xi + u)^2} + \mathcal{O}(\ln^{-4}\xi)\,, \tag{6.20}$$

where u is an action dependent constant ($u \approx 1.3$ for the standard action (2.12)), ξ is the infinite volume correlation length and the coefficient f_1 is universal and thus can be obtained from the sine Gordon model, where

also a LWW coupling can be defined and the following expansion holds for large $p = \frac{8\pi}{8\pi - \beta_{\mathrm{sG}}^2}$:

$$\bar{g}^2_{\mathrm{sG}}(ML, p) = \bar{g}^2(ML, \infty) + \frac{2f_1(ML)}{p^2} + \mathcal{O}(p^{-4}) \tag{6.21}$$

The measurements are made on a series of n lattices with different resolutions a/L. If ML would be held fixed the solid lines in figure 6.2, which correspond to equation (6.20), should be recovered.

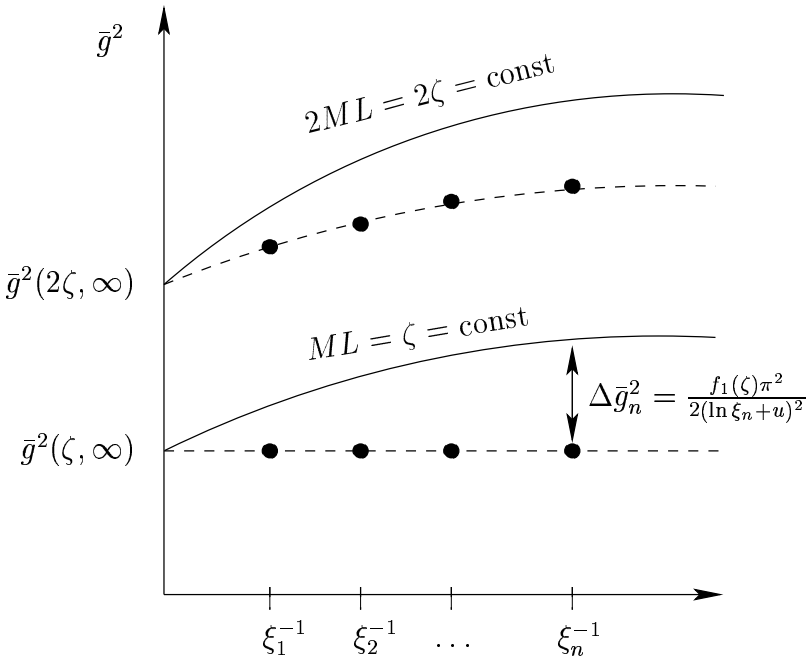

Figure 6.2: Calculation of lattice artifacts for the step scaling function

In order to measure the step scaling function for all lattices the bare coupling β_i (i_{th} lattice) is tuned to keep the coupling $2M(L)L = \bar{g}^2(\zeta, \infty)$ constant (lower dashed line in the figure). The infinite volume correlation lengths ξ_i are determined by the β_i. Thus this line is not at a fixed $ML = \zeta$ - the corresponding values are $ML = z_i = \zeta + \Delta z_i$. The difference between these two lines is given by eq. (6.20): $\Delta\bar{g}_i^2 = -\frac{f_1(\zeta)\pi^2}{2(\ln \xi_i + u)}$. Assuming that $\Delta\bar{g}_i^2$ is small, Δz_i can be obtained from:

$$\Delta z_i \approx \frac{f_1(\zeta)\pi^2}{2(\ln \xi_i + u)^2} \frac{1}{\frac{\partial \bar{g}^2}{\partial z}\big|_{z=\zeta}} \tag{6.22}$$

To obtain the lattice step scaling function for each lattice the lattice size is doubled at a fixed β_i and the coupling is measured again:

$$\Sigma(2, \bar{g}^2(\zeta, \infty), \xi_i) = \bar{g}^2(2z_i, \xi_i) \tag{6.23}$$

One obtains the upper dashed line in the figure. The lattice artifacts for this step scaling function can be approximated:

$$\begin{aligned}
\Sigma(2,\bar{g}^2(\zeta,\infty),\xi_i) &= \bar{g}^2(2\zeta+2\Delta z_i,\xi_i) \\
&\approx \bar{g}^2(2\zeta,\xi_i)+2\Delta z_i \frac{\partial\bar{g}^2}{\partial z}\Big|_{z=2\zeta} \\
&\approx \bar{g}^2(2\zeta,\infty)-\frac{f_1(2\zeta)\pi^2}{2(\ln\xi_i+u)^2}+\frac{f_1(\zeta)\pi^2}{(\ln\xi_i+u)^2}\frac{\frac{\partial\bar{g}^2}{\partial z}\big|_{z=2\zeta}}{\frac{\partial\bar{g}^2}{\partial z}\big|_{z=\zeta}} \\
&= \Sigma(2,\bar{g}^2(\zeta,\infty),\infty)+\frac{d\pi^2}{2(\ln\xi_i+u)^2}+\ldots \qquad (6.24)
\end{aligned}$$

with d given by:

$$d=-f_1(2\zeta)+2f_1(\zeta)\frac{\frac{\partial\bar{g}^2}{\partial z}\big|_{z=2\zeta}}{\frac{\partial\bar{g}^2}{\partial z}\big|_{z=\zeta}} \qquad (6.25)$$

The corrections to (6.24) are of order $\mathcal{O}(\ln^{-4}\xi_i)$. The required slopes can be obtained approximately from numerical solutions of the DdV equation. The coefficient f_1 can be obtained from a numerical solution of the sine Gordon version of the DdV equations. Instead of using the XY model specific integral kernel (5.21) the version (5.19) with finite p has to be used.

Chapter 7

Results

7.1 Summary of the results

The lattice step scaling function Σ was measured for three values of the LWW-coupling at different lattice spacings with Monte Carlo methods. After an extrapolation to continuum the results were compared with values obtained from solutions of the DdV equation.

The extrapolations to the continuum were done using the formula:

$$\Sigma(2, u, \xi) = \sigma(2, u) + \frac{c}{(\ln \xi + 1.3)^2}\,, \tag{7.1}$$

where u is the value of the LWW-coupling and ξ is the infinite volume correlation length in lattice units. When the continuum is approached, ξ diverges and can be obtained from the Kosterlitz Thouless prediction:

$$\xi = A \exp\left(C \left| \frac{\beta_c - \beta}{\beta_c} \right|^{-\frac{1}{2}} \right) \tag{7.2}$$

The non universal constants are known with good precision for the standard action [19]:

$$A = 0.223 \pm 0.013 \tag{7.3}$$

$$C = 1.78 \pm 0.02 \tag{7.4}$$

This behavior is an excellent approximation to the exact correlation lengths near the critical point. Moreover small deviations are suppressed by taking the logarithm.

The first observation is that indeed the lattice artifacts decay in the predicted way. When the lattice step scaling function $\Sigma(2, u, \xi)$ is plotted against $(1.3 + \ln \xi)^{-2}$, a linear dependence is observed. The desired values c and $\sigma(2, u)$ can be obtained from a linear fit (fig. 7.1 - 7.3). The Monte Carlo results are in very good agreement with the continuum predictions within

numerical precision. At this point I cannot say whether the predicted values for the constant c are fully confirmed or not. The errors are large, and also the theoretical value can only be calculated approximatively. Table 7.1 summarizes the results. The values listed are:

u: The value of the LWW-coupling at which the step scaling function was measured.

σ_{DdV}: The step scaling function obtained from solutions of the DdV equation.

σ_{MC}: The step scaling function obtained from a continuum extrapolation of Monte Carlo data.

c_{th}: A prediction for the slope of the linear fit (according to eq. (6.24)).

c_{MC}: The slope of the linear fit.

$\chi^2/_{\mathrm{dof}}$: A measure for the quality of the fit.

The constant c_{th} was not calculated for the last point. It corresponds to $ML \approx 2.2 \times 10^{-12}$, where the iteration procedure converges very slowly and it is difficult to obtain solutions of the DdV equation, especially for $p < \infty$ where the Fourier transformation (5.19) cannot be carried out exactly.

u	$\sigma_{\mathrm{DdV}}(2,u)$	$\sigma_{\mathrm{MC}}(2,u)$	c_{th}	c_{MC}	$\chi^2/_{\mathrm{dof}}$
3.0038	4.3895	4.40 ± 0.02	3.596	2.4 ± 0.7	2.42/3
1.7865	1.8282	1.829 ± 0.007	5.321	4.7 ± 0.5	0.66/3
1.602	1.6029	1.608 ± 0.004		4.3 ± 0.5	0.83/3

Table 7.1: Comparison of theoretical predictions with numerical results.

Another method to validate the predictions is to force the linear fit to go through the predicted continuum value and check whether the resulting $\chi^2/_{\mathrm{dof}}$ values are acceptable (fig. 7.4). Following this method the results in table 7.2 were obtained. Again the predictions from solutions of the DdV equation are confirmed: $\chi^2/_{\mathrm{dof}} < 1$ for all points.

u	$\sigma_{\mathrm{DdV}}(2,u)$	$\chi^2/_{\mathrm{dof}}$
3.0038	4.3895	2.79/4
1.7865	1.8282	0.68/4
1.602	1.6029	2.71/4

Table 7.2: Comparison of theoretical predictions with numerical results.

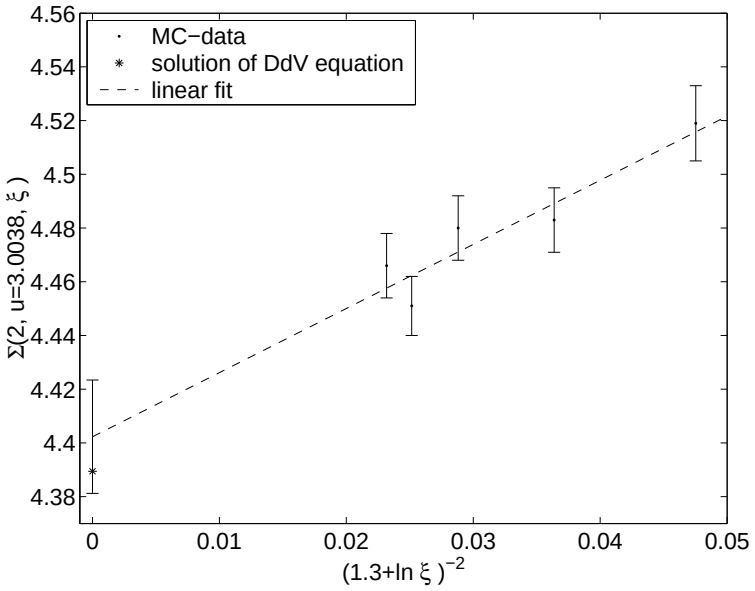

Figure 7.1: Comparison of MC-data with a numerical solution of the DdV equation. The spatial extents L/a of the lattices were 20, 40, 80, 120 and 160 in order of increasing ξ.

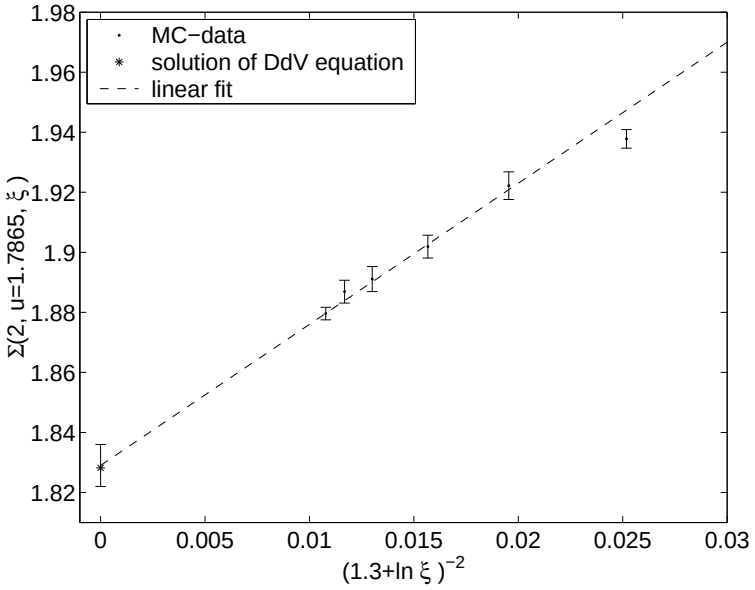

Figure 7.2: Comparison of MC-data with a numerical solution of the DdV equation. The spatial extents L/a of the lattices were 10, 20, 40, 80, 120 and 160. The smallest lattice was discarded in the fit.

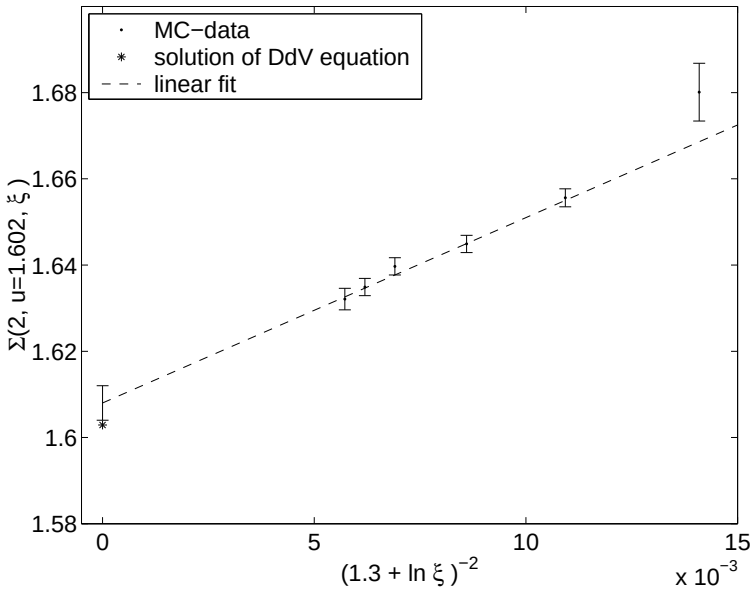

Figure 7.3: Comparison of MC-data with a numerical solution of the DdV equation. The spatial extents L/a of the lattices were 10, 20, 40, 80, 120 and 160. The smallest lattice was discarded in the fit.

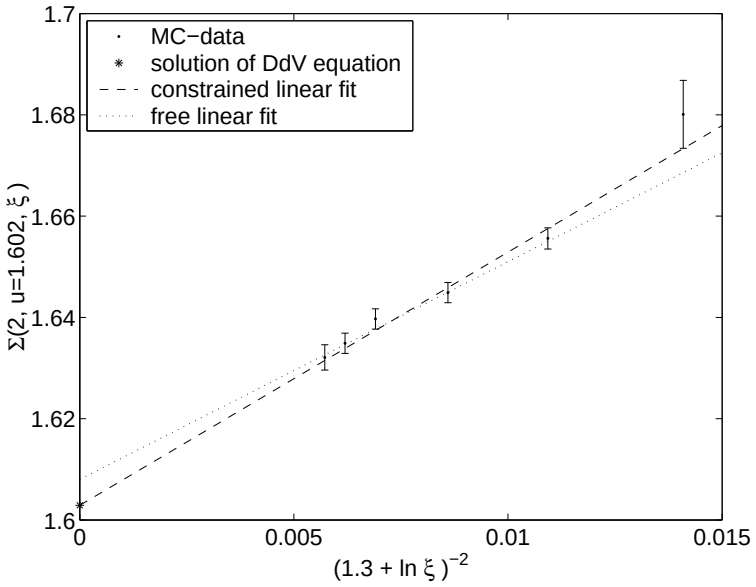

Figure 7.4: Comparison of MC-data with a numerical solution of the DdV equation. The spatial extents L/a of the lattices were 10, 20, 40, 80, 120 and 160. The smallest lattice was discarded in the fits.

In the appendices B.1 and B.2 all the data is collected that was needed to extract this results.

7.2 Conclusions and outlook

This thesis has lead to two main results:

- The predicted universal form of leading lattice artifacts in the XY model has been confirmed by numerical simulations for the step scaling function.

- Exact results for the continuum step scaling function in the context of the sine Gordon model have been compared with results obtained from lattice simulations of the XY model. They have been found to be in very good agreement within the numerical precision.

The first point can be regarded as another confirmation of the Kosterlitz Thouless scenario. Calculations leading to this scenario are more or less approximative and there has been a controversy whether they can be trusted or not for a long time [46]. This result demonstrates in an impressive way, how important it is to have detailed knowledge of the functional form of lattice artifacts in order to extract meaningful continuum values. Although the accessible range of lattices was much bigger than it would be for example in four dimensional theories, an extrapolation to the continuum would lead to wrong results if the lattice artifacts were not known (fig. 7.5).

The second result gives strong evidence that all the considerations and assumptions leading from the six-vertex model via Bethe ansatz to a set of integral equations that can be used to calculate the energy spectrum of the $O(2)$ nonlinear $\sigma-$model are correct. Simultaneously it brings some more light into the nature of the QFT that is obtained from the massive continuum limit of the XY model.

Some points that would be worth looking at in more detail are:

- Investigate whether non standard lattice artifacts occur in other systems (e.g. $O(n > 2)$ nonlinear $\sigma-$models).

- Reproduce the results in the context of a different model that also exhibits a Kosterlitz Thouless phase transition (e.g. The SOS model dual to the Villain model).

- Check whether a different physical observable than the LWW-coupling can be extracted from the theoretical predictions and confront it with results from lattice simulations.

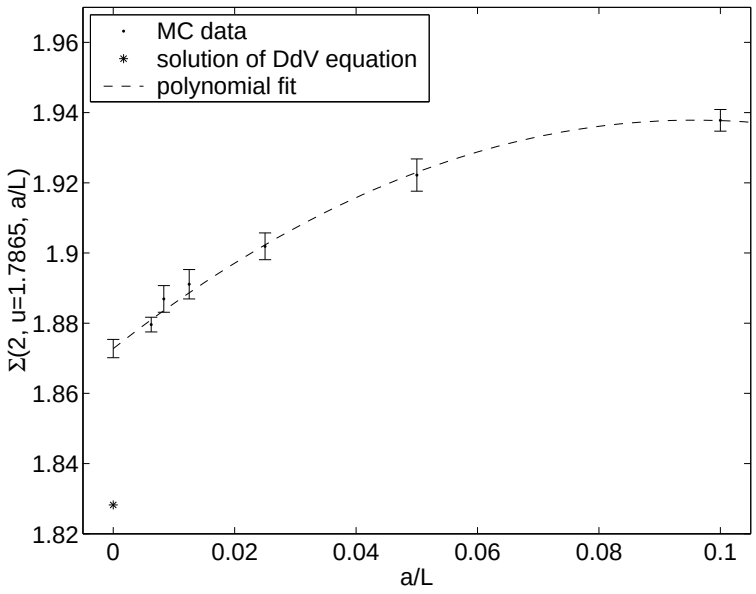

Figure 7.5: Comparison of MC-data with a numerical solution of the DdV equation. The predicted continuum value could not have been confirmed, if power like lattice artifacts $\propto (a/L)^2 + c(a/L) + d$ were assumed.

Acknowledgments

I wish to thank the computational physics group at the Humboldt university for creating an enjoyable working atmosphere and supporting me throughout the work. My special gratitude goes to Prof. U. Wolff who formulated this interesting task and to Dr. F. Knechtli. They were always willing to share their knowledge and experience with me. To Dr. J. Balog I am grateful for his detailed answers to my emails. Last but not least I want to thank my family.

Appendix A

Proofs and additional calculations

A.1 The Villain bond

Applying Poisson's summation formula 3.39 on 3.30 yields:

$$\begin{aligned} z_V(\theta) &= \sum_{m=-\infty}^{+\infty} \exp\left[-\frac{\beta}{2}(\theta - 2\pi m)^2\right] \\ &= \sum_{n=-\infty}^{+\infty} \int_{-\infty}^{+\infty} d\phi \ \exp\left[-\frac{\beta}{2}(\theta - 2\pi\phi)^2 + i2\pi n\phi\right] \\ &= \sum_{n=-\infty}^{+\infty} \int_{-\infty}^{+\infty} d\phi \ \exp\left[-\frac{\beta}{2}\theta^2 + 2\beta\left(\frac{\theta + \frac{in}{\beta}}{2}\right)^2\right] \\ &\qquad \cdot \exp\left[-2\pi^2\beta\left(\phi - \frac{\theta + \frac{in}{\beta}}{2\pi}\right)^2\right] \end{aligned} \tag{A.1}$$

After a change of variables this Gaussian integral can be performed which leads to the desired result:

$$z_V = (2\pi\beta)^{-\frac{1}{2}} \sum_{n=-\infty}^{+\infty} \exp\left[in\theta - \frac{n^2}{2\beta}\right] \tag{A.2}$$

A.2 Proof of detailed balance for the single cluster algorithm

The probability to activate the link (create a bond) between sites x and y is:

$$p_{\vec{r}}(\vec{s}_x, \vec{s}_y) = 1 - e^{\min[0,\ -2\beta\vec{s}_x\cdot\vec{r}\ \ \vec{s}_y\cdot r]} \tag{A.3}$$

Consequently the probability for gaining a bond configuration $B \subset \Lambda \times \Lambda$ starting at a spin configuration S with a certain $\vec{r}$ is:

$$w_{\vec{r},S}(B) = \prod_{<x,y>\in B} p_{\vec{r}}(\vec{s}_x, \vec{s}_y) \prod_{<x,y>\notin B} (1 - p_{\vec{r}}(\vec{s}_x, \vec{s}_y)) \tag{A.4}$$

Different bond configurations can lead to the same cluster, so the total probability for gaining the cluster C with the single cluster algorithm is

$$P_{\vec{r},S}(C) = \frac{|C|}{|\Lambda|} \sum_{\substack{B \\ C(B)=C}} \prod_{<x,y>\in B} p_{\vec{r}}(\vec{s}_x, \vec{s}_y) \prod_{<x,y>\in \partial C} (1 - p_{\vec{r}}(\vec{s}_x, \vec{s}_y)) \tag{A.5}$$

Where $|C|$ is the size of the cluster (number of sites). $|C|/|\Lambda|$ is the probability for a randomly chosen site to belong to the cluster. The summation runs over all bond configurations that result in the same cluster. The second product extends over all links $\{x, y\}$ where $x \in C$ and $y \notin C$. Now detailed balance can be proved:

$$\frac{W(S \to S')}{W(S' \to S)} = \frac{\int_{S_1} d\vec{r} \sum_{C\in\mathcal{P}} P_{\vec{r},S}(C)\ \delta[S', R_{\vec{r},C}(S)]}{\int_{S_1} d\vec{r} \sum_{C\in\mathcal{P}} P_{\vec{r},S'}(C)\ \delta[S, R_{\vec{r},C}(S')]}\,, \tag{A.6}$$

where the integral extends over all unit Vectors in $\mathbb{R}^2$ and the δ-functional is defined by:

$$\left(\prod_{x\in\Lambda} \int_{S_1} d\vec{s}_x\right)\ \delta[S, S']\ F[S] = F[S']. \tag{A.7}$$

$\mathcal{P}$ is the set of all possible clusters. If C^* is the set of sites where in equation (A.6) S differs from S' and $\vec{r}^*$ is the vector normal to the plane at which all spins $\vec{s}_x$

with $x \in C^*$ have to be reflected to get S' then:

$$\begin{aligned}
\frac{W(S \to S')}{W(S' \to S)} &\overset{1}{=} \frac{\frac{|C^*|}{|\Lambda|}\left(\sum_{\substack{B \\ C(B)=C^*}} \prod_{<x,y>\in B} p_{\vec{r}^*}(\vec{s}_x, \vec{s}_y) \prod_{<x,y>\in \partial C^*} (1 - p_{\vec{r}^*}(\vec{s}_x, \vec{s}_y))\right)}{\frac{|C^*|}{|\Lambda|}\left(\sum_{\substack{B \\ C(B)=C^*}} \prod_{<x,y>\in B} p_{\vec{r}^*}(\vec{s}_x\,', \vec{s}_y\,') \prod_{<x,y>\in \partial C^*} (1 - p_{\vec{r}^*}(\vec{s}_x\,', \vec{s}_y\,'))\right)} \\
&= \prod_{<x,y>\in \partial C^*} \frac{1 - p_{\vec{r}^*}(\vec{s}_x, \vec{s}_y)}{1 - p_{\vec{r}^*}(\vec{s}_x\,', \vec{s}_y\,')} \\
&\overset{3}{=} \prod_{<x,y>\in \partial C^*} e^{\min(0,-2\beta \vec{s}_x \cdot \vec{r}^*\, \vec{s}_y \cdot \vec{r}^*) - \min(0,-2\beta \vec{s}_x\,' \cdot \vec{r}^*\, \vec{s}_y\,' \cdot \vec{r}^*)} \\
&= \prod_{<x,y>\in \partial C^*} e^{\min(0,-2\beta \vec{s}_x \cdot \vec{r}^*\, \vec{s}_y \cdot \vec{r}^*) - \min(0,2\beta \vec{s}_x \cdot \vec{r}^*\, \vec{s}_y \cdot \vec{r}^*)} \\
&= \prod_{<x,y>\in \partial C^*} e^{-2\beta \vec{s}_x \cdot \vec{r}^*\, \vec{s}_y \cdot \vec{r}^*} \\
&= \prod_{<x,y>\in \partial C^*} e^{-\beta(2\vec{s}_x \cdot \vec{r}^*\, \vec{s}_y \cdot \vec{r}^* + \vec{s}_x \cdot \vec{s}_y - \vec{s}_x \cdot \vec{s}_y)} \\
&= \prod_{<x,y>\in \partial C^*} e^{-\beta(\vec{s}_x \cdot \vec{s}_y - [\vec{s}_x - 2(\vec{s}_x \cdot \vec{r}^*)\vec{r}^*] \cdot \vec{s}_y)} \\
&= \prod_{<x,y>\in \partial C^*} e^{-\beta(\vec{s}_x \cdot \vec{s}_y - \vec{s}_x\,' \cdot \vec{s}_y)} \\
&= \prod_{<x,y>\in \partial C^*} e^{-\beta(\vec{s}_x \cdot \vec{s}_y - \vec{s}_x\,' \cdot \vec{s}_y\,')} \\
&= \prod_{<x,y>} e^{-\beta(\vec{s}_x \cdot \vec{s}_y - \vec{s}_x\,' \cdot \vec{s}_y\,')} \qquad \text{(A.8)}
\end{aligned}$$

Exchanging the spin $\vec{s}_x$ with its reflected version (on the plane perpendicular to $\vec{r}$) in $\vec{s}_x \cdot \vec{r}$ only changes the sign. That was used in steps one and three. In the last steps it was used that the dot product is invariant under the reflection of both spins.

A.3 Variance of an improved estimator

$$\begin{aligned}
\langle A^2 \rangle &= \frac{1}{Z} \int D\theta\ D\psi\ \exp(-H(\theta,\psi)) A(\theta,\psi)^2 \\
&\overset{2}{=} \frac{1}{Z} \int D\theta\ \frac{\int D\psi\ \exp(-H(\theta,\psi)) A(\theta,\psi)^2}{\int D\psi'\ \exp(-H(\theta,\psi'))} \int D\psi'\ \exp(-H(\theta,\psi')) \\
&\geq \frac{1}{Z} \int D\theta\ \left(\frac{\int D\psi\ \exp(-H(\theta,\psi)) A(\theta,\psi)}{\int D\psi'\ \exp(-H(\theta,\psi'))}\right)^2 \int D\psi'\ \exp(-H(\theta,\psi')) \\
&= \langle A_{\text{imp}}^2 \rangle \\
\Rightarrow \qquad \langle A^2 \rangle - \langle A \rangle^2 &\geq \langle A_{\text{imp}}^2 \rangle - \langle A_{\text{imp}} \rangle^2 \qquad \text{(A.9)}
\end{aligned}$$

In the second step it was taken advantage of: $\langle A^2\rangle_{\text{cond}} \geq \langle A\rangle^2_{\text{cond}}$, in the last step $\bar{A} = \langle A\rangle = \langle A\rangle_{\text{imp}}$ was subtracted on both sides.

A.4 Performing the integrals for $\tilde{X}_{11}(t, t+1)$ and $\tilde{X}_{22}(t, t+1)$

The $O(2)$ in two dimensions can be parametrized by:

$$\int dX\ \mathbf{X} = \int_0^{2\pi} d\phi \begin{pmatrix} \cos\phi & -\sin\phi \\ \sin\phi & \cos\phi \end{pmatrix} \tag{A.10}$$

Now the integrals in $z(t, t+1)$ can be calculated:

$$\begin{aligned} z(t,t+1) &= \int_0^{2\pi} d\phi\, e^{(Q_{11}+Q_{22})\cos\phi + (Q_{21}-Q_{12})\sin\phi} \\ &= \int_0^{2\pi} d\phi\, \exp\left[\kappa \sin\left(\arctan\frac{Q_{11}+Q_{22}}{Q_{21}-Q12} + \phi\right)\right] \\ &= 2\pi I_0(\kappa) \end{aligned} \tag{A.11}$$

Where I_0 is a modified Bessel function and

$$\kappa = \sqrt{(Q_{11}+Q_{22})^2 + (Q_{21}-Q_{12})^2}. \tag{A.12}$$

So the desired result is:

$$\begin{aligned} \tilde{X}_{11}(t,t+1) &= \tilde{X}_{22}(t,t+1) \\ &= \frac{1}{z(t,t+1)} \int_0^{2\pi} d\phi\, e^{(Q_{11}+Q_{22})\cos\phi + (Q_{21}-Q_{12})\sin\phi} \cos\phi \\ &= \frac{1}{z(t,t+1)} \frac{Q_{11}+Q_{22}}{\kappa} \int_0^{2\pi} d\phi\, \exp\left[\kappa \sin\left(\arctan\frac{Q_{11}+Q_{22}}{Q_{21}-Q12} + \phi\right)\right] \\ &\qquad \cdot \sin\left(\arctan\frac{Q_{11}+Q_{22}}{Q_{21}-Q12} + \phi\right) \\ &= \frac{Q_{11}+Q_{22}}{\kappa} \frac{I_1(\kappa)}{I_0(\kappa)} \end{aligned} \tag{A.13}$$

$\langle X_{12}(t, t+1)\rangle$ and $\langle X_{21}(t, t+1)\rangle$ are calculated analogously.

A.5 Calculation of $\left\langle e^{-\beta\Delta H}\right\rangle$

$$\begin{aligned}\left\langle e^{-\beta\Delta H}\right\rangle &= \frac{1}{Z}\sum_{S} e^{-\beta H(S)} \sum_{S'} T(S\to S') e^{-\beta(H(S')-H(S))} \\ &= \frac{1}{Z}\sum_{S,S'} T(S\to S') e^{-\beta H(S')} \\ &= \frac{1}{Z}\sum_{S'} e^{-\beta H(S')} \sum_{S} T(S'\to S) \\ &= \frac{1}{Z}\sum_{S'} e^{-\beta H(S')} \\ &= 1 \end{aligned} \tag{A.14}$$

A.6 η independence of the DdV equation

In the integrals for the energy levels and in the nonlinear integral equations, the way of integration is shifted by η into the imaginary direction of the complex plane. If the way of integration Ω looks as follows:

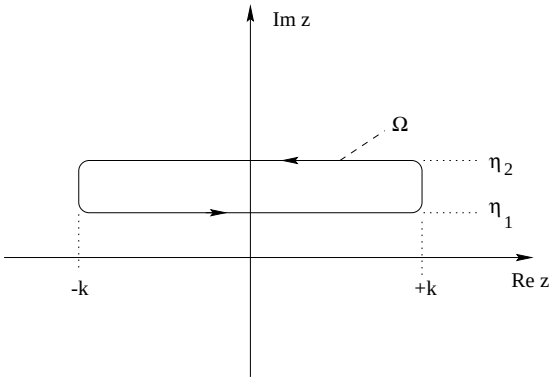

Figure A.1: Integration contour Ω

Cauchy's integral formula

$$\oint_{\Omega} dz\ f(z) = 0, \tag{A.15}$$

can be applied if $f(z)$ is analytic in the region enclosed by Ω. If for $k\to\infty$, $f(\pm k)$ approaches zero, the segments perpendicular to the real axis in Ω can be neglected:

$$\int_{-\infty+i\eta_1}^{+\infty+i\eta_1} dz\ f(z) - \int_{-\infty+i\eta_2}^{+\infty+i\eta_2} dz\ f(z) = 0 \tag{A.16}$$

Therefore $\int_{-\infty}^{+\infty} dz\ f(z+i\eta)$ is independent of η as long as no poles are crossed when the way of integration is shifted. All integrands that are treated in section 5.2 are analytic in the region $0 < \eta < \pi$.

This considerations are valid in the continuum. The η-independence is only approximative, when the integrals are compactified and discretized. But the *cut* and the number of sampling points were chosen large enough, to make the η dependence smaller then the desired precision goal (of about 8 significant digits).

Appendix B

Tables

B.1 The step scaling function

In the following tables results for the step scaling function at different LWW-couplings and lattice spacings are listed. The quantities mentioned in the table are:

L/a: Spatial extent in lattice units.

β: Bare coupling.

$\bar{g}^2(L,\beta)$: LWW-coupling.

$\Sigma(2,u,L/a)$: Lattice step scaling function.

$\frac{\partial\Sigma}{\partial\bar{g}^2}\big|_u$: Rough estimate for the slope of the step scaling which is needed to calculate the errors.

$\Sigma_{cor}(2,u,L/a)$: Lattice step scaling function after correction of the systematic error. The error was calculated according to (6.16).

The calculations that were necessary to find the correct value of the bare coupling are summarized in appendix B.2.

L/a	β	$\bar{g}^2(L,\beta)\approx u$	$\Sigma(2,u,L/a)$	$\frac{\partial\Sigma}{\partial\bar{g}^2}\big\|_u$	$\Sigma_{cor}(2,u,L/a)$
20	0.9649	3.0022(45)	4.5144(74)	2.5	4.519(14)
40	1.0	3.0036(41)	4.4824(75)	2.4	4.483(12)
80	1.0241	3.0146(39)	4.5055(76)	2.4	4.480(12)
120	1.0359	2.9919(39)	4.4232(64)	2.3	4.451(11)
160	1.0423	3.0069(38)	4.4742(64)	2.5	4.466(12)

Table B.1: $\bar{g}^2(L)$ and $\Sigma(2,\bar{g}^2(L),L/a)=\bar{g}^2(2L)$ at different L/a and $\bar{g}^2\approx 3.0038$

L/a	β	$\bar{g}^2(L,\beta) \approx u$	$\Sigma(2,u,L/a)$	$\frac{\partial\Sigma}{\partial\bar{g}^2}\big\vert_u$	$\Sigma_{cor}(2,u,L/a)$
10	1.0358	1.7866(16)	1.9379(19)	1.3	1.9378(31)
20	1.0541	1.7837(16)	1.9161(19)	2.2	1.9222(46)
40	1.0668	1.7860(16)	1.9010(19)	1.8	1.9019(38)
80	1.0756	1.7896(16)	1.8973(19)	2.0	1.8911(42)
120	1.0800	1.7882(17)	1.8898(19)	1.7	1.8869(38)
160	1.0830	1.7850(16)	1.8778(13)	1.2	1.8796(21)

Table B.2: $\bar{g}^2(L)$ and $\Sigma(2,\bar{g}^2(L),L/a) = \bar{g}^2(2L)$ at different L/a and $\bar{g}^2 \approx 1.7865$

L/a	β	$\bar{g}^2(L,\beta) \approx u$	$\Sigma(2,u,L/a)$	$\frac{\partial\Sigma}{\partial\bar{g}^2}\big\vert_u$	$\Sigma_{cor}(2,u,L/a)$
10	1.0720	1.5971(12)	1.6721(66)	1.6	1.6801(67)
20	1.0825	1.6033(12)	1.6574(13)	1.4	1.6556(21)
40	1.0903	1.6032(12)	1.6463(14)	1.2	1.6449(20)
80	1.096	1.6020(11)	1.6397(13)	1.4	1.6397(20)
120	1.0984	1.6034(13)	1.6365(14)	1.1	1.6349(20)
160	1.1	1.6028(13)	1.6330(13)	1.2	1.6321(25)

Table B.3: $\bar{g}^2(L)$ and $\Sigma(2,\bar{g}^2(L),L/a) = \bar{g}^2(2L)$ at different L/a and $\bar{g}^2 \approx 1.602$

B.2 The LWW-coupling

The following table summarizes the simulations that were necessary to calculate the step scaling function. $L \times K$ denotes the size of the lattice (in lattice units).

Table B.4: $\bar{g}^2$ at different lattice sizes $L \times K$ and bare couplings β

$L \times K$	β	$\bar{g}^2$
10×50	1.082	1.5565 ± 0.0011
	1.0722	1.5967 ± 0.0012
	1.0720	1.5971 ± 0.0012
	1.0451	1.7313 ± 0.0015
	1.0368	1.7807 ± 0.0015
	1.0356	1.7864 ± 0.0015
	1.0358	1.7866 ± 0.0016
	1.00	2.0269 ± 0.0019
20×100	1.1085	1.4809 ± 0.0021
	1.0865	1.5821 ± 0.0012
	1.0826	1.6014 ± 0.0012
	1.0825	1.6033 ± 0.0012
	1.0824	1.6047 ± 0.0012
	1.0823	1.6040 ± 0.0012

Table B.4: continuation

$L \times K$	β	$\bar{g}^2$
	1.0820	1.6057 ± 0.0012
	1.0722	1.6645 ± 0.0013
	1.072	1.6721 ± 0.0066
	1.0551	1.7768 ± 0.0015
	1.0543	1.7838 ± 0.0016
	1.0541	1.7837 ± 0.0016
	1.0451	1.8548 ± 0.0017
	1.0368	1.9306 ± 0.0019
	1.0358	1.9379 ± 0.0019
	1.0356	1.9391 ± 0.0018
	1.0	2.3599 ± 0.0030
	0.977	2.7570 ± 0.0079
	0.9649	3.0022 ± 0.0045
	0.962	3.0755 ± 0.0041
	0.956	3.2155 ± 0.0045
	0.88	5.9798 ± 0.0091
	0.87	6.460 ± 0.011
	0.82	9.2838 ± 0.0079
	0.70	17.928 ± 0.019
	0.65	22.175 ± 0.026
	0.58	28.734 ± 0.036
40×200	1.0865	1.6287 ± 0.0013
	1.1085	1.5039 ± 0.0021
	1.1	1.5434 ± 0.0022
	1.0920	1.5910 ± 0.0012
	1.0903	1.6032 ± 0.0012
	1.0902	1.6058 ± 0.0012
	1.0918	1.5933 ± 0.0012
	1.0826	1.6563 ± 0.0013
	1.0825	1.6574 ± 0.0013
	1.0823	1.6584 ± 0.0014
	1.0722	1.7365 ± 0.0014
	1.0670	1.7830 ± 0.0015
	1.0668	1.7860 ± 0.0016
	1.0658	1.7938 ± 0.0015
	1.0551	1.9012 ± 0.0019
	1.0543	1.9188 ± 0.0019
	1.0541	1.9161 ± 0.0018
	1.0531	1.9317 ± 0.0020
	1.034	2.1961 ± 0.0048
	1.0	3.0036 ± 0.0041
	0.991	3.3145 ± 0.0052
	0.977	3.892 ± 0.013
	0.9649	4.5144 ± 0.0074
	0.962	4.6719 ± 0.0075
	0.956	5.0290 ± 0.0082
	0.87	12.657 ± 0.069
	0.85	14.829 ± 0.011
	0.82	18.480 ± 0.014
	0.80	21.062 ± 0.029
	0.75	28.100 ± 0.044

Table B.4: continuation

$L \times K$	β	$\bar{g}^2$
	0.70	35.774 ± 0.068
	0.58	57.415 ± 0.020
80×400	1.105	1.5423 ± 0.0011
	1.1	1.5762 ± 0.0024
	1.0969	1.5954 ± 0.0012
	1.0960	1.6020 ± 0.0011
	1.0920	1.6320 ± 0.0013
	1.0918	1.6355 ± 0.0013
	1.0903	1.6463 ± 0.0014
	1.0902	1.6465 ± 0.0013
	1.0824	1.6558 ± 0.0014
	1.0823	1.6584 ± 0.0014
	1.082	1.6585 ± 0.0013
	1.0766	1.7798 ± 0.0016
	1.0756	1.7896 ± 0.0016
	1.07554	1.7906 ± 0.0018
	1.0755	1.7912 ± 0.0016
	1.0754	1.7944 ± 0.0016
	1.0670	1.8994 ± 0.0021
	1.0668	1.9010 ± 0.0019
	1.0658	1.9147 ± 0.0019
	1.057	2.0612 ± 0.0042
	1.05	2.1976 ± 0.0054
	1.045	2.3112 ± 0.0059
	1.034	2.6290 ± 0.0062
	1.0241	3.0146 ± 0.0039
	1.0217	3.1301 ± 0.0041
	1.02	3.2157 ± 0.0047
	1.0	4.4824 ± 0.0075
	0.991	5.2313 ± 0.0087
	0.87	12.657 ± 0.0692
	0.85	29.663 ± 0.028
	0.84	32.204 ± 0.074
	0.80	42.09 ± 0.12
	0.75	56.61 ± 0.28
	0.65	44.37 ± 0.11
120×600	1.105	1.5545 ± 0.0011
	1.1	1.5876 ± 0.0024
	1.0984	1.6034 ± 0.0013
	1.0983	1.6043 ± 0.0012
	1.098	1.6065 ± 0.0013
	1.081	1.7794 ± 0.0017
	1.0805	1.7798 ± 0.0017
	1.08	1.7882 ± 0.0017
	1.0798	1.7916 ± 0.0014
	1.057	2.2031 ± 0.0052
	1.045	2.5790 ± 0.0054
	1.0359	2.9919 ± 0.0039
	1.034	3.0942 ± 0.0044
	1.0	6.169 ± 0.021
	0.9	28.365 ± 0.028

Table B.4: continuation

$L \times K$	β	$\bar{g}^2$
160×800	1.11	1.5324 ± 0.0024
	1.105	1.5642 ± 0.0012
	1.1	1.6014 ± 0.0026
	1.1	1.6028 ± 0.0013
	1.0969	1.6290 ± 0.0013
	1.0960	1.6397 ± 0.0013
	1.0849	1.7619 ± 0.0016
	1.084	1.7722 ± 0.0016
	1.0835	1.7773 ± 0.0016
	1.083	1.7850 ± 0.0016
	1.0828	1.7872 ± 0.0016
	1.0756	1.8973 ± 0.0019
	1.07554	1.8973 ± 0.0019
	1.0755	1.9005 ± 0.0019
	1.0754	1.8938 ± 0.0022
	1.0746	1.9121 ± 0.0019
	1.057	2.3555 ± 0.0059
	1.05	2.6226 ± 0.0031
	1.045	2.8619 ± 0.0034
	1.0423	3.0069 ± 0.0038
	1.0241	4.5055 ± 0.0076
	1.0217	4.7888 ± 0.0080
	1.02	4.9873 ± 0.0087
	1.0	8.0543 ± 0.043
	0.84	63.54 ± 0.46
240×1200	1.105	1.5772 ± 0.0013
	1.1	1.6190 ± 0.0026
	1.0984	1.6365 ± 0.0014
	1.0983	1.6387 ± 0.0014
	1.098	1.6431 ± 0.0013
	1.081	1.8746 ± 0.0017
	1.0805	1.8811 ± 0.0019
	1.08	1.8898 ± 0.0019
	1.0798	1.8955 ± 0.0019
	1.057	2.6185 ± 0.0063
	1.045	3.462 ± 0.011
	1.0359	4.4232 ± 0.0064
	1.034	4.6783 ± 0.0075
	0.9	56.92 ± 0.17
320×1600	1.105	1.5871 ± 0.0012
	1.1	1.6330 ± 0.0013
	1.084	1.8617 ± 0.0017
	1.0835	1.8701 ± 0.0019
	1.083	1.8778 ± 0.0013
	1.0828	1.8830 ± 0.0018
	1.081	1.9218 ± 0.0018
	1.05	3.5220 ± 0.0048
	1.045	4.1093 ± 0.0060
	1.0423	4.4742 ± 0.0064

B.3 Approaching the continuum at β_c

The following table lists values of the LWW coupling on different lattices $L \times 5L$ at $\beta = \beta_c$.

L	$\bar{g}^2(L)$
10	1.41720 ± 0.00092
20	1.43350 ± 0.00086
40	1.44878 ± 0.00096
80	1.46062 ± 0.00090
120	1.46698 ± 0.00096
160	1.47008 ± 0.00099
240	1.4772 ± 0.0010
320	1.4808 ± 0.0011
480	1.4841 ± 0.0010

Table B.5: $\bar{g}^2(L, a/L)$ at $\beta = \beta_c \approx 1.1197$

B.4 Parameters needed to calculate the lattice artifacts

To calculate the lattice artifacts for the step scaling function according to eq. (6.24) the slopes of the LWW-coupling and the constants f_1 must be known. The following table summarizes the values that were obtained from solutions of the DdV equations. Two different values of f_1 are listed. The first at $p = 40$ and the other at $p = 60$. The difference comes from the $\mathcal{O}(p^{-4})$ correction to eq. (6.21).

ζ	$\bar{g}^2(\zeta)$	$g^2(2\zeta)$	$f_1(\zeta)$	$f_1(2\zeta)$	$\frac{\partial \bar{g}^2}{\partial z}\big\vert_{\zeta}$	$\frac{\partial \bar{g}^2}{\partial z}\big\vert_{2\zeta}$
0.014024	1.78650	1.82821	1.9607	1.6435	3.6428	2.5233
			1.9681	1.6482		
0.9652	3.00384	4.38946	0.2528	−0.0921	1.2759	1.5859
			0.2562	−0.0919		
2.1917×10^{-12}	1.60202	1.60288				

Table B.6: Parameters needed to calculate the lattice artifacts.

Selbständigkeitserklärung

Hiermit erkläre ich, die vorliegende Arbeit selbständig ohne fremde Hilfe verfaßt und nur die angegebene Literatur und Hilfsmittel verwendet zu haben.

Tomasz Korzec
31. Januar 2003

Bibliography

[1] J. M. Kosterlitz and D. J. Thouless, J. Phys. **C6**, 1181 (1973).

[2] M. Lüscher, P. Weisz, and U. Wolff, Nucl. Phys. **B359**, 221 (1991).

[3] J. Balog, J. Phys. **A34**, 5237 (2001), hep-lat/0011078.

[4] J. Balog, Kosterlitz-Thouless theory and LWW coupling in the two-dimensional O(2) nonlinear sigma model, talk given at the HU on 27 november 2001.

[5] Muon g-2, G. W. Bennett *et al.*, Phys. Rev. Lett. **89**, 101804 (2002), hep-ex/0208001.

[6] A. M. Polyakov, Phys. Lett. **B59**, 79 (1975).

[7] J. Balog *et al.*, Nucl. Phys. **B618**, 315 (2001), hep-lat/0106015.

[8] R. P. Feynman and A. R. Hibbs, *Quantum mechanics and path integrals* (McGraw-Hill, 1965).

[9] K. Symanzik, Nucl. Phys. **B226**, 187 (1983).

[10] K. Symanzik, DESY 79/76.

[11] M. Hasenbusch, P. Hasenfratz, F. Niedermayer, B. Seefeld, and U. Wolff, Nucl. Phys. Proc. Suppl. **106**, 911 (2002), hep-lat/0110202.

[12] J. Cardy, *Scaling and Renormalization in Statistcal Physics* (Cambridge University Press, 1996).

[13] V. L. Berezinskii, Soviet Phys. JETP **34 No. 3**, 610 (1972).

[14] L. Kadanoff, *Statistical Physics, Statics, Dynamics and Renormalization* (World Scientific, 1999).

[15] N. D. Mermin and H. Wagner, Phys. Rev. Lett. **17**, 1133 (1966).

[16] F. Spitzer, *Principles of Random Walk* (Princeton: Van Nostrand, 1964), pp. 148–151.

[17] J. M. Kosterlitz, J. Phys. C **7**, 1046 (1974).

[18] J. Villain, J. Phys. (France) **36**, 581 (1975).

[19] M. Hasenbusch, M. Marcu, and K. Pinn, Physica **A208**, 124 (1994), hep-lat/9404016.

[20] M. Hasenbusch and K. Pinn, J. Phys. **A30**, 63 (1997), cond-mat/9605019.

[21] D. J. Amit, Y. Y. Goldschmidt, and G. Grinstein, J. Phys. **A13**, 585 (1980).

[22] S. T. Chui and P. A. Lee, Phys. Rev. Lett. **35**, 315 (1975).

[23] S. Samuel, Phys. Rev. **D18**, 1916 (1978).

[24] S. R. Coleman, Phys. Rev. **D11**, 2088 (1975).

[25] D. R. Nelson and K. J. M., Phys. Rev. Lett. **39**, 1201 (1977).

[26] E. Webster, G. Webster, and M. Chester, Phys. Rev. Lett. **42**, 243 (1979).

[27] S. L. Adler, Phys. Rev. **D23**, 2905 (1981).

[28] R. G. Edwards, S. J. Ferreira, J. Goodman, and A. D. Sokal, Nucl. Phys. **B380**, 621 (1992), hep-lat/9112002.

[29] P. W. Kasteleyn and F. C. M., J. Phys. Soc. Jpn. Suppl. **26s** (1969).

[30] R. H. Swendsen and J.-S. Wang, Phys. Rev. Lett. **58**, 86 (1987).

[31] U. Wolff, Phys. Rev. Lett. **62**, 361 (1989).

[32] F. Niedermayer, (1996), hep-lat/9704009.

[33] J. Hoshen and R. Kopelman, Phys. Rev. **B14**, 3438 (1976).

[34] U. Wolff, Nucl. Phys. **B322**, 759 (1989).

[35] M. Hasenbusch, Nucl. Phys. Proc. Suppl. **42**, 764 (1995).

[36] R. Baxter, *Exactly solved models in statistical mechanics* (Academic Press, London, 1982).

[37] A. B. Zamolodchikov, Physics reviews **vol. 2**, 1 (1990).

[38] H. Bethe, Z. Phys. **71**, 205 (1931).

[39] C. Destri and H. J. de Vega, Phys. Rev. Lett. **69**, 2313 (1992).

[40] D. Fioravanti, A. Mariottini, E. Quattrini, and F. Ravanini, Phys. Lett. **B390**, 243 (1997), hep-th/9608091.

[41] C. Destri and H. J. de Vega, Nucl. Phys. **B504**, 621 (1997), hep-th/9701107.

[42] G. Feverati, F. Ravanini, and G. Takács, Phys. Lett. **B430**, 264 (1998), hep-th/9803104.

[43] F. Ravanini, (2000), hep-th/0102148, Lectures given at Eotvos Summer School in Physics.

[44] M. Lüscher, Commun. Math. Phys. **104**, 177 (1986).

[45] J. Balog, private communication.

[46] A. Luther and D. J. Scalpino, Phys. Rev. **B16**, 1153 (1977).